TUNGSTEN PRODUCTION BY ELECTRODEOXIDATION

A THESIS SUBMITTED TO
THE GRADUATE SCHOOL OF NATURAL AND APPLIED SCIENCES
OF
MIDDLE EAST TECHNICAL UNIVERSITY

BY

METEHAN ERDOĞAN

IN PARTIAL FULFILLMENT OF THE REQUIREMENTS
FOR
THE DEGREE OF MASTER OF SCIENCE
IN
METALLURGICAL AND MATERIALS ENGINEERING

JANUARY 2007

Approval of the Graduate School of Natural and Applied Sciences

_____

Prof. Dr. Canan ÖZGEN
Director

I certify that this thesis satisfies all the requirements as a thesis for the degree of Master of Science

_____

Prof. Dr. Tayfur Öztürk
Head of Department

This is to certify that we have read this thesis and that in our opinion it is fully adequate, in scope and quality, as a thesis for the degree of Master of Science

_____

Prof. Dr. İshak Karakaya
Supervisor

Examining Committee Members:

Prof. Dr. Ahmet GEVECİ (METU, METE) _____

Prof. Dr. İshak KARAKAYA (METU, METE) _____

Prof. Dr. Naci SEVİNÇ (METU, METE) _____

Prof. Dr. Tayfur ÖZTÜRK (METU, METE) _____

Assist. Prof.Dr. Hasan OKUYUCU (G.U., Met. Edu.) _____

I hereby declare that all information in this document has been obtained and presented in accordance with academic rules and ethical conduct. I also declare that, as required by these rules and conduct, I have fully cited and referenced all material and results that are not original to this work.

Metehan ERDOĞAN

Signature:

ABSTRACT

TUNGSTEN PRODUCTION BY ELECTRODEOXIDATION

Erdoğan, Metehan

M.S., Department of Metallurgical and Materials Engineering
Supervisor: Prof. Dr. İshak Karakaya
January 2007, 65 pages

There has been some efforts to produce tungsten by electrolytic reduction. Among various electrolytic methods, reduction of tungsten compounds in molten salt electrolytes seems to be promising. Thermodynamic computations and experimental studies were performed to shed some light over this method. Experimental studies involved electrochemical reduction of solid tungsten compounds; tungsten trioxide (WO_3) and calcium tungstate ($CaWO_4$), in the form of an assembled cathode of porous pellets attached to a current collector. Molten calcium chloride ($CaCl_2$) and a molten equimolar mixture of calcium chloride and sodium chloride ($CaCl_2$ - NaCl) were used as the electrolytes. Reduced samples were characterised by means of X-ray diffraction analyses. The results of these analyses, supported with thermodynamic computations, showed that WO_3 cannot be reduced electrochemically at high temperatures without loss, because it reacts with $CaCl_2$ by liberating volatile tungsten oxychloride (WO_2Cl_2). In electrochemical reduction of $CaWO_4$, X-ray diffraction results indicated the presence of significant concentrations of calcium compounds in addition to tungsten. Metallic tungsten was obtained after treating

reduced samples with dilute hydrochloric acid solutions. In addition to these, analytical studies were performed to infer the theoretical potential for the reduction reaction and electroreduction pathway.

Keywords: Tungsten, Electrolysis, Molten Salt, Electrodeoxidation

ÖZ

TUNGSTENİN ELEKTRODEOKSİDASYON YÖNTEMİYLE ÜRETİMİ

Erdoğan, Metehan

Yüksek Lisans, Metalurji ve Malzeme Mühendisliği Bölümü

Tez Yöneticisi: Prof. Dr. İshak Karakaya

Ocak 2007, 65 Sayfa

Tungstenin elektrolitik indirgeme yoluyla üretimine yönelik bir dizi çalışma yapılmıştır. Çeşitli elektolitik yöntemler arasından, tungsten bileşiklerinin ergimiş tuz çözeltileri içerisinde indirgenmesi gelecek vaad etmektedir. Bu olaya biraz ışık tutabilmek amacıyla, termodinamik hesaplamalar ve deneysel çalışmalar yapılmıştır. Deneysel çalışmalar, iletken bir telin ucuna tutturulmak suretiyle hücrenin katotunu oluşturan, gözenekli yapılar halindeki katı tungsten bileşikleri; tungsten trioksit (WO_3) ve kalsiyum tungstatın ($CaWO_4$), elektrokimyasal yöntemlerle indirgenmesini esas almıştır. Elektrolit olarak, ergimiş haldeki kalsiyum klorür ($CaCl_2$) ve eşit mol sayıda kalsiyum klorür ve sodyum klorür (NaCl) içeren tuz çözeltileri kullanılmıştır. İndirgenen örneklerin içeriği, X-ışınları kırınımı analizleri aracılığıyla belirlenmiştir. Termodinamik hesaplamalar ile desteklenen bu analizler, tungsten trioksitin, yüksek sıcaklıklarda kayıp vermeksizin indiregenemeyeceğini ortaya koymuştur, çünkü; WO_3, $CaCl_2$ ile uçucu bir madde olan tungsten oksiklorür (WO_2Cl_2) çıkışıyla sonuçlanan bir reaksiyona girmektedir. $CaWO_4$'ün elektrokimyasal indirgenmesine gelindiğinde ise, X-ışınları kırınımı sonuçları, indirgenen örneklerde tungstenin yanısıra önemli miktarlarda kalsiyum bileşikleri

bulunduğunu göstermiştir. Metalik tungsten, indirgenen örneklerin seyreltik hidroklorik asit (HCl) çözeltilerine tabi tutulmaları sonucu elde edilmiştir. Bunlara ek olarak, indirgenme reaksiyonunun teorik potansiyelini ve elektrokimyasal indirgenme mekanizmasını bulmaya yönelik analitik çalışmalar yapılmıştır.

Anahtar Kelimeler: Tungsten, Elektroliz, Ergimiş Tuz, Elektrodeoksidasyon

To My Family & Sevgi,

ACKNOWLEDGEMENTS

I would like to express my deepest gratitude to my supervisor Prof. Dr. İshak Karakaya for his great guidance, advice, criticism, encouragements, patience and insight throughout the research.

My special thanks go to Dr. Nurşen Koç whose benevolent methodological explanations and advises on different topics related to my research were particularly important for me and have to be highly appreciated. I would like to thank cordially to Prof. Dr. Muharrem Timuçin, Prof. Dr. Ahmet Geveci, Prof. Dr. Yavuz Topkaya and Prof. Dr. Naci Sevinç for providing material and support at essential times. The technical assistance and suggestions of İsa Hasar, Necmi Avcı, Cengiz Tan, Cemal Yanardağ and Atalay Özdemir are also gratefully acknowledged.

I am grateful to the late Özgün Yılmazok, Osman Kılıç, Pınar Karpuz and especially Meltem Yıldız for the care with which they helped me prepare this thesis; and for conversations that clarified my thinking on this and other matters. Their friendship and professional collaboration meant a great deal to me.

A number of colleagues allowed me to use some of their materials and made comments that encouraged me to revise and improve my studies. In this regard, I am indebted to İlker Özcan, Gökhan Demirci, Yankı Başaran, Semih Sunkar, Barış Okatan and Ziya Esen.

And - last but by no means least! - I am deeply indebt to my parents, my brother and my sister-in-law for their never-ending love and spiritual support at critical and opportune times.

As always it was Sevgi who provided the shelter conditions under which the work could take place: thanks to her for this and many other things.

TABLE OF CONTENTS

ABSTRACT ..... **iv**

ÖZ ..... **vi**

ACKNOWLEDGEMENTS ..... **ix**

TABLE OF CONTENTS ..... **x**

LIST OF TABLES ..... **xii**

LIST OF FIGURES ..... **xiii**

1. INTRODUCTION **1**

1.1 Properties of Tungsten *1*

1.2 Uses of Tungsten *1*

1.3 History of Tungsten *4*

1.4 Economy of Tungsten *6*

1.5. Raw Materials of Tungsten *7*

2. LITERATURE REVIEW **10**

2.1 Industrial Production *10*

2.2 Disadvantages of the Current Process and Alternative Processes *13*

2.3 FFC Cambridge Process *16*

2.4 The Objective of This Research *22*

3. EXPERIMENTAL 23

3.1 Experimental Setup 23

3.1.1 Cell Assembly 23

3.1.2 Auxiliary Apparatus 25

3.2 Experimental Procedure 27

3.2.1 Cell Feed Preparation 27

3.2.2 Cell Operation 32

4. RESULTS AND DISCUSSION 35

4.1 Electrolysis of Tungsten Trioxide (WO_3) 35

4.2 Electrolysis of Calcium Tungstate ($CaWO_4$) 40

4.2.1 Experimental Procedure and Results 40

4.2.2 Effect of Sintering 42

4.2.3 Determination of Theoretical Potential for the Reduction Reaction 44

4.2.3.1 Experiments at Applied Constant Potential 45

4.2.3.2 Experiments at Applied Constant Current 51

4.2.4 Determination of Electroreduction Pathway 53

4.2.5 Isolation of Tungsten 58

5. CONCLUSION 61

REFERENCES 63

LIST OF TABLES

Table 1.1: Some of the Important Properties of Tungsten [1] 2

Table 1.2: Formulas and %WO_3 Contents of Wolframite and Scheelite [8] 8

Table 4.1: List of Calculated Values 47

Table 4.2: List of Calculated Values 50

Table 4.3 : List of Calculated Values 52

Table 4.4: Tafel Coefficients for Anodic Overvoltage on Graphite in Cryolite Melts for Two Different Temperatures [35] 57

LIST OF FIGURES

Figure 1.1: Primary Consumption Sectors by End Uses Depending on Different Regions of the World [2].....3

Figure 1.2: World Mine Production of Tungsten in 2003 [4].....4

Figure 1.3: Tungsten World Production in years 1910-1996 (Repr. from [5]) 6

Figure 1.4: Tungsten Price (LBM quotation) versus Time (1960-1995) (Startup and closure dates of some of the mines are also marked, repr. from [6].).....7

Figure 1.5: Annual Averages of Tungsten Prices between 1997 and 2005 (Reproduced from [7]) 8

Figure 1.6: Estimated World Reserves of Tungsten in Different Countries [9] (CIS=Community of Independent States).....9

Figure 2.1: Flowsheet of APT Production from the Ore [11] (Arrows between the two columns indicate alternative roots) 11

Figure 2.2: Tungsten Production from APT (Most of the metal is then used in the manufacture of tungsten carbides [12]).....12

Figure 2.3: Ellingham Diagram for Metal-Metal Oxide Systems (W-WO_3 line is in blue and H_2-H_2O line is in red, reproduced from [13]).....15

Figure 2.4: Cell Arrangement of Cathodic Refining Technique.....19

Figure 2.5: Two different cell arrangements of FFC Cambrige process. In the upper one, a wire is used as the current collector. In the lower one, crucible itself is made the current collector. 21

Figure 3.1: Schematic Drawing of the Cell Assembly 24

Figure 3.2: Schematic Drawing of the Auxiliary Apparatus 26

Figure 3.3: A view of the experimental setup 27

Figure 3.4: X-ray Diffraction Spectrum of the Sample after Complete Conversion to $CaWO_4$ 28

Figure 3.5: Flowchart of Pellet Preparation Procedure 30

Figure 3.6: Approximate equilibrium diagram for the $CaCl_2$-H_2O system at an HCl partial pressure of 10^{-3} atm. showing possible phase boundaries between the hydrates and the solution. The $Ca(OH)_2$ is off scale at the lower left. Reproduced from [28]. 31

Figure 3.7: Equilibrium diagram for the NaCl-H_2O system at an HCl partial pressure of 10^{-3} atm. Reproduced from [28]. 31

Figure 3.8: Phase diagram of $CaCl_2$-NaCl system (Reproduced from [29]) 33

Figure 3.9: Recorded voltage values ($E_{\text{electrical connections}}$) as a function of applied current (I), obtained by short-circuiting the electrodes in a molten Pb pool at 600°C. 33

Figure 4.1: X-ray diffraction spectrum of the deposited yellow powder. The major phase is WO_2Cl_2. 36

Figure 4.2: X-ray diffraction spectrum of the sample taken from the cathode. The major phase is tungsten. 36

Figure 4.3: Result of thermodynamic equilibrium calculations by F*A*C*T program under the conditions of the experimental work [30]…….. 38

Figure 4.4: Voltage versus Time Graph at a Constant Applied Current Value of 2.5 A..... 39

Figure 4.5:Current versus Time Graph at a Constant Potential Value of 3.4 V . 39

Figure 4.6:$CaCl_2$-$CaWO_4$ Phase Diagram (Reproduced from [31]) 41

Figure 4.7: X-ray diffraction spectrum of one of the experiments with $CaWO_4$ pellet in $CaCl_2$-NaCl molten eutectic mixture. Products are W, $CaCO_3$ and $Ca(OH)_2$..... 42

Figure 4.8: Current vs. Time Graphs of the Experiments (Higher current values were recorded with the unsintered pellet.) 43

Figure 4.9: X-ray diffraction spectrum of a sample (sintered at 1200°C) after 400 minutes of electrolysis. The sample was taken from the surface..... 43

Figure 4.10: X-ray diffraction spectrum of a sample (sintered at 1200°C) after 400 minutes of electrolysis. The sample was taken from the interior parts of the pellet. 44

Figure 4.11: I vs. t Curves of Electrolysis of $CaWO_4$ Pellets at Different Applied Constant Voltages..... 46

Figure 4.12: Variation of Current Values with Net Cell Potential (Extrapolation of the regression line gives $E_{reaction}+\eta$, and the slope of the line gives $R_{pellet}+R_{electrolyte}$.) 47

Figure 4.13: Photograph of A Partially Reduced Sample (Black regions are the reduced portions, whereas white regions are the unreduced portions of the pellet.). 48

Figure 4.14: E_{net} vs. I Curve for the Initial Periods of the Experiments (Slope of the regression line gives the resistance of the electrolyte.) 50

Figure 4.15: Observed Potential Values As a Function of Time at Different Applied Constant Current Values 51

Figure 4.16: Observed Potential Values As A Function of Electrical Charge at Different Applied Constant Current Values 52

Figure 4.17: T vs. η Graph Obtained for an Anodic Current Density of 0.1 $A.cm^{-2}$ (Extrapolation of regression curve to 600°C gives an η value of 1.1 V.) 58

Figure 4.18: X-ray diffraction spectrum of a sample after an experiment in which the vessel was flushed with argon gas……...……..... 60

Figure 4.19: X-ray Diffraction Spectrum of a Sample after 0.2 M HCl Solution Treatment 60

CHAPTER 1

INTRODUCTION

1.1 Properties of Tungsten

Tungsten (W), with atomic number 74, is in the 6th group of the periodic table with chromium and molybdenum. It closely resembles molybdenum in all its properties. Tungsten has the highest melting point of all metals (3422∓20° C). It has the lowest coefficient of thermal expansion, exceptional high density, very high thermal creep resistance, good high-temperature mechanical properties, very high moduli of compression and elasticity. It also has good conductivity for heat and electricity. Some of the important properties of tungsten are given in Table 1.1 [1].

Tungsten is a shiny white metal and can easily be processed when in its purest form. Usually, however, it contains small concentrations of carbon and oxygen, which give tungsten metal its considerable hardness and brittleness. Most of these unusual properties are due to the half-filled 5d electron shells with a very high binding energy of the tungsten in the bcc crystal arising from the strong, unsaturated covalent bonds. Based on these properties, tungsten, tungsten alloys and some tungsten compounds cannot be substituted in many important applications in different fields of modern technology.

1.2 Uses of Tungsten

Because of the properties given in section 1.1, metallic tungsten has been used for many technical applications. Hardmetals also called as cemented carbides,

Table 1.1: Some of the Important Properties of Tungsten [1]

Atomic Number	74
Average Relative Atomic Mass	183.85±0.03
Electron Configuration	[Xe] $4f^{14}$ $5d^{4}$ $6s^{2}$
Crystal Structure	Body-Centered Cubic A2
Lattice Parameter	a=3.16524 Å (298 K)
Atomic radius (metallic)	137 pm
Density	19.25 g/cm^{3} (298 K)
Melting Point	3422±15°C
Vapor Pressure (2000°C)	8.15×10^{-8} Pa
Boiling Point	5700±200 °C
Specific heat capacity	135 $J \cdot kg^{-1} \cdot K^{-1}$ (298 K)
Enthalpy of fusion	46 $kJ \cdot mol^{-1}$
Enthalpy of sublimation	~860 $kJ \cdot mol^{-1}$
Coefficient of Thermal Expansion	$4.32\text{-}4.68 \times 10^{-6} \cdot K^{-1}$ (298 K)
Electrical Resistivity	5.28 μΩ·cm
Thermal Conductivity Coefficient	1.75 $\cdot W \cdot cm^{-1} \cdot K^{-1}$(298K)
Modulus of Elasticity	390-410 GPa (298K)
Hardness	300-650 HV30

are the main end use application for tungsten. Cemented carbides are composites in which carbide particles are cemented by a binder matrix. Therefore they combine the high hardness and strength of the tungsten carbide (WC) with the toughness and plasticity of a metallic binder (Co, Ni, and Fe). The second important consumption area is the use of tungsten as the alloying element in iron and steel industry. Tungsten, as a carbide-forming element, increases strength, hardness, wear resistance and toughness of the steel. It finds uses in stainless, tool, heat resisting and full alloy steels as well as superalloys. The use of tungsten in iron and steel industry lost its supremacy gradually over time, especially with the growing market of hardmetals. Nevertheless, steel industry is today still the second largest tungsten consumer. Tungsten mill products,

especially used in lamp industry and for electric and electronic contacts, are another important usage of the metal. Tungsten compounds are also in use for chemical applications and products such as catalysts, pigments, paints and lubricants. Finally, tungsten metal is also required for some other special applications such as vacuum metallizing and substituting poisonous lead and tungsten oxides in smart windows and optical glasses. Figure 1.1 [2] demonstrates the shares of main tungsten consumers.

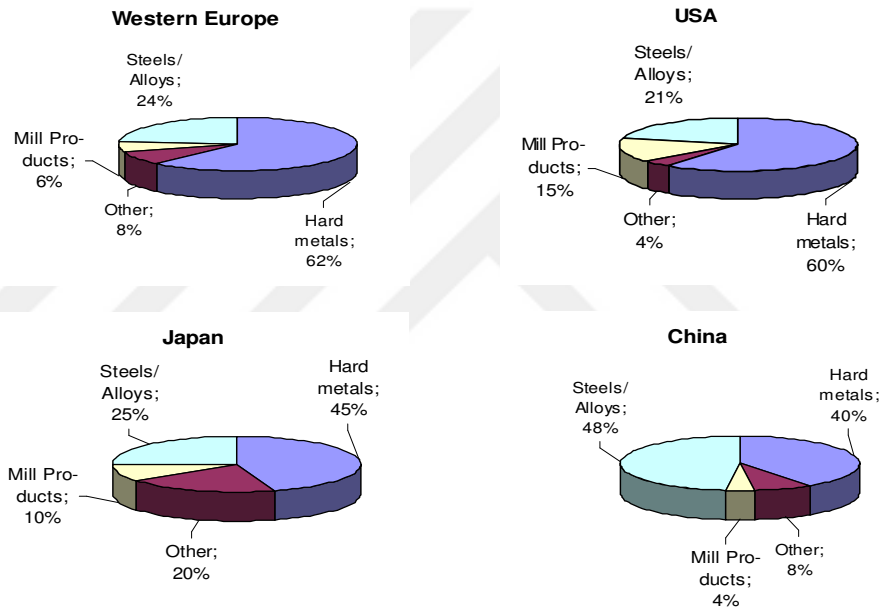


Figure 1.1: Primary Consumption Sectors by End Uses Depending on Different Regions of the World [2]

China is now the largest user of tungsten. Next in order of magnitude is the USA, followed by Japan, and then Russia. Other countries account for less than 10% of the total consumption [3]. However, at the same time, China is by far the largest mine producer of tungsten in the world. Figure 1.2 [4] demonstrates world mine production of tungsten in year 2003.

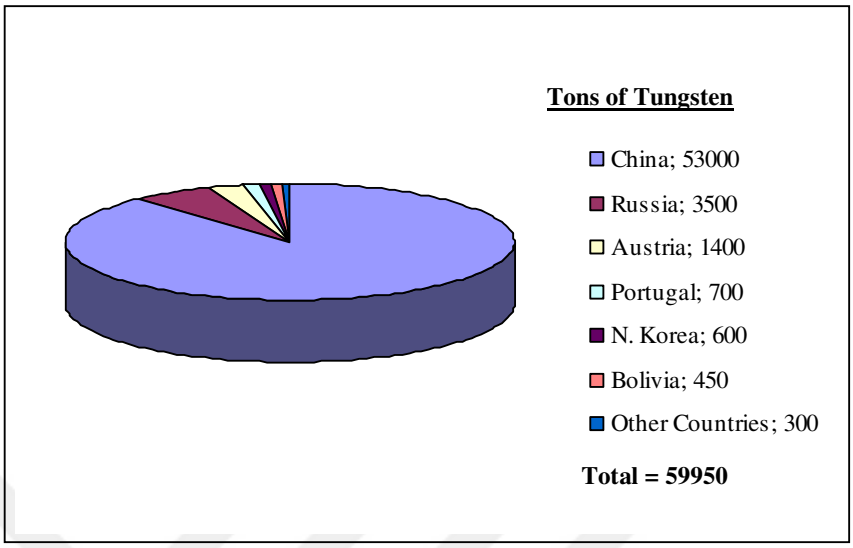


Figure 1.2: World Mine Production of Tungsten in 2003 [4]

1.3 History of Tungsten

The history of tungsten goes back to the 17th century when it was noticed that certain ores disturbed the reduction of cassiterite (a tin mineral) and induced slagging. The miners gave these ores German nicknames like "wolfert" and "wolffram" (which means wolf froth). Then in 1758, Axel Fredrik Cronstedt, discovered and described an unusually heavy mineral that he called "tung-sten", which is Swedish for heavy stone. In 1781 Carl Wilhelm Scheele succeeded in isolating the oxide (tungsten trioxide). Torbern Bergman predicted that the acid isolated by Scheele contains a new metal which should be possible to prepare by coal reduction. A Spanish nobleman, Don Juan Jose de Elhuyar and his brother Fausto de Elhuyar de Suvisa were the first in 1783 to prepare tungsten metal by the method suggested by Bergman. They named it wolfram. Jöns Jacob Berzelius (1816) and later also Friedrich Wöhler (1824) described the oxides and bronzes of tungsten. While Wolfram established itself in Germany and

Scandinavia, the Anglo-Saxon countries preferred Cronstedt's "tungsten". In 1821, K.C. von Leonhard proposed the name "Scheelite" for the mineral $CaWO_4$.

In 1847, R. Oxland took out a patent for the manufacture of sodium tungstate and tungstic acid, which forms the starting point of the metallurgy of tungsten. Oxland can be considered to be the real founder of the tungsten chemistry.

The early attempts to produce steels containing tungsten were made by J. Jacob and F. Koeller (Reichraming steel works; Austria) in 1855. Tests of this steel demonstrated a very fine silky grain, good weldability, and a significantly increased tensile strength at moderate toughness. Further improvements in alloying and hardening of steels by tungsten were made late in the 19th century (Robert Mushet special steel; Boehler "Boreas"steel). Rapid growth and widespread application followed the invention, and the launch of high speed steels by Bethlehem Steel (F.W. Taylor and M. White) took place in 1900 at the Paris World Exhibition.

The second important breakthrough in tungsten applications was made by W. D. Coolidge in 1908/1909. Coolidge succeeded in preparing a ductile tungsten wire by thermomechanical processing. Metal powder was pressed to bars, sintered and forged to thin rods. Very thin wire was then drawn from these rods. This was the beginning of tungsten powder metallurgy, which was instrumental in the rapid development of the lamp industry.

The year 1923 is the next important milestone in the chronology of tungsten. It marks the invention of hardmetals (combining WC and Cobalt by liquid phase sintering) by K. Schröter and the corresponding application for a patent which was granted to Osram Studiengesellschaft in Berlin and licensed to Krupp in Essen in 1926. Nowadays, hardmetals (cemented carbides) are the main application for tungsten.

1.4 Economy of Tungsten

Figure 1.3 illustrates the growth in tungsten production between the years 1910 and 1996 [5]. Except for temporary fluctuations, a steady growth due to increasing industrialization in the world can be observed. War times were always related to maxima and economical recessions to minima. Tungsten's economy was generally ruled by the supply/demand situation, which itself was a consequence of the world's general economic situation. Booming industry was always associated with enhanced tungsten consumption and mine production as well as with the search for new deposits. Times of general recession always showed minimum of the consumption combined with mine closures. Wars reflected situations of highest industrial activity and always maximum of consumption and prices. Tungsten prices in between 1960-1995 together with startup and closure dates of some of the mines can be seen in Figure 1.4 [6].

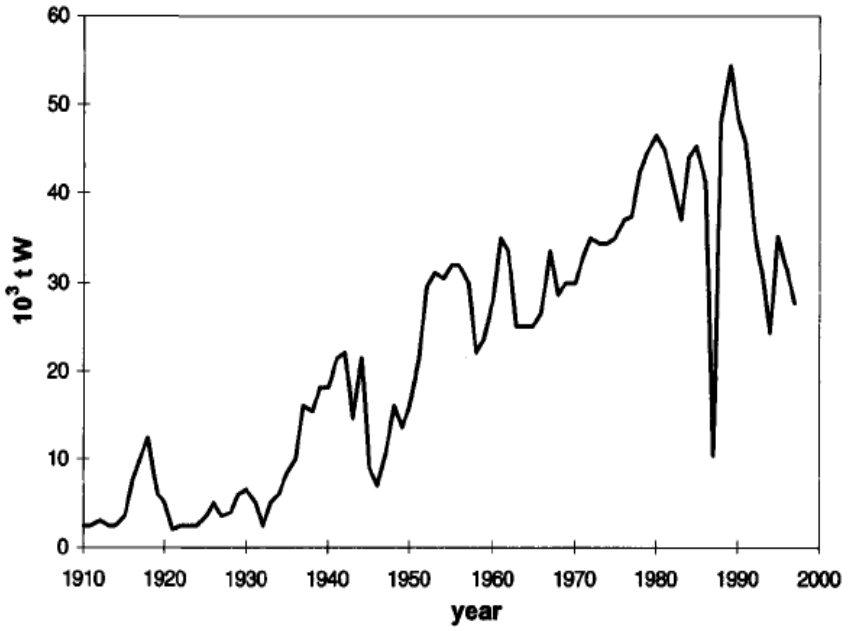


Figure 1.3: Tungsten World Production in years 1910-1996 (Reproduced from [5])

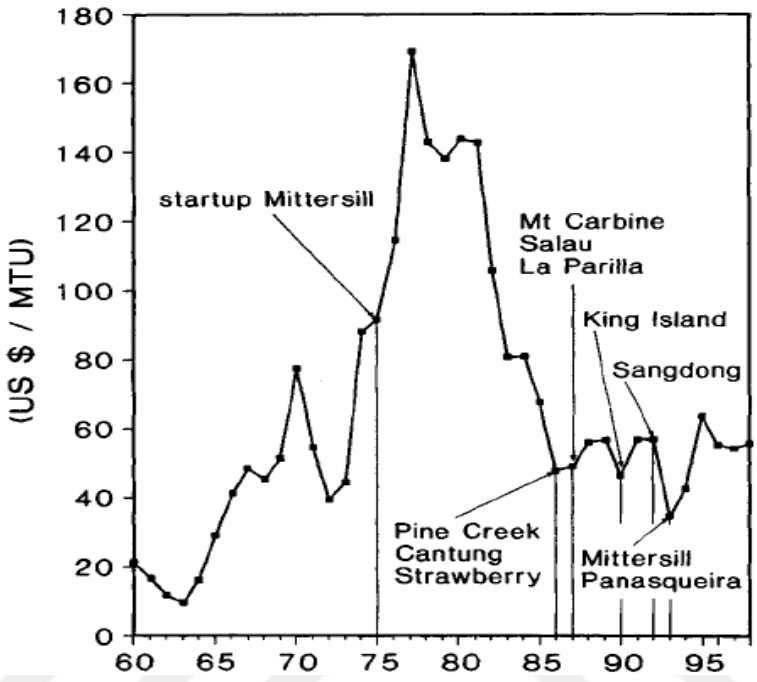


Figure 1.4: Tungsten Price (LBM quotation) versus Time (1960-1995) (Startup and closure dates of some of the mines are also marked, reproduced from [6].)

Recent tungsten price fluctuations are given in Figure 1.5 [7]. As it can be seen from this figure, tungsten prices have increased significantly in 2005, from a level of 65-95 US$/MTU in 2004 to 280 US$/MTU in mid-2005. Prices are generally quoted per metric ton unit ("MTU" - one hundredth of a metric ton of 1,000 kilograms) of contained tungsten trioxide (WO_3). One MTU contains 10 kilograms of tungsten trioxide (WO_3) and/or 7.93 kilograms of tungsten (W).

1.5. Raw Materials of Tungsten

The main raw materials used in tungsten production are tungsten ore concentrates. Tungsten ores are considered to be commercial if they contain over 0.2% WO_3 or equivalent. Although more than thirty tungsten bearing

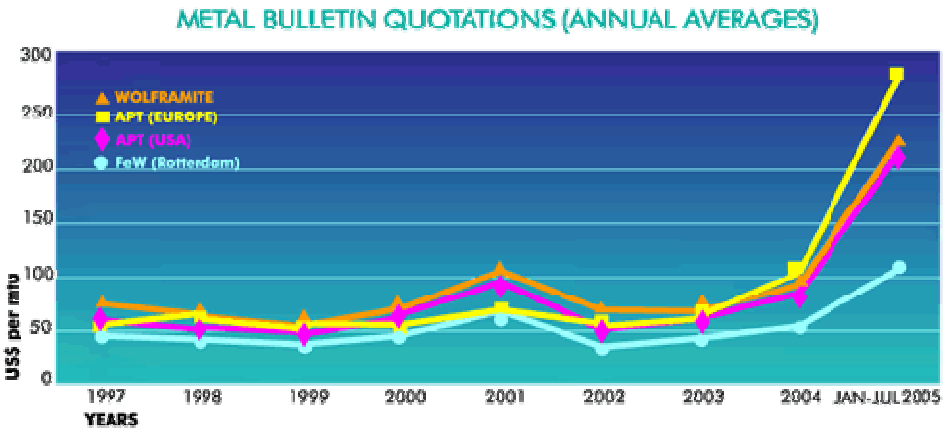


Figure 1.5: Annual Averages of Tungsten Prices between 1997 and 2005 (Reproduced from [7])

minerals are known, however, only two of them are important for industrial use; wolframite and scheelite. Table 1.2 shows formulas and $\%WO_3$ contents of wolframite and scheelite [8].

Table 1.2: Formulas and $\%WO_3$ Contents of Wolframite and Scheelite [8]

Name	Formula	$\%WO_3$
Wolframite	$(Fe, Mn)WO_4$	76.5
Scheelite	$CaWO_4$	80.5

Pure scheelite has blue-white fluorescence in ultraviolet light, a property which is utilized in prospecting. Wolframite is a general term for iron and manganese tungstates where the iron/manganese ratio can vary. A mineral with more than 80% $FeWO_4$ is called Ferberite and a mineral with more than 80% $MnWO_4$ is called Hübnerite.

Most tungsten ores contain less than 1.5% WO_3 and ore dressing plants are always in close proximity to the mine. The ore is first crushed and milled to liberate the tungsten mineral crystals. Scheelite ore can be concentrated by

gravimetric methods, often combined with froth flotation, whilst wolframite ore can be concentrated by gravity, sometimes in combination with magnetic separation. Ore concentrates in international trading require 65-75% WO_3.

Estimated tungsten reserves (W content) of the world are about 7 million tonnes, including reserves which so far are not economically workable. A further estimate suggests that 70% of the reserves are scheelite and 30% of the reserves are wolframite ores. It is predicted that these reserves will last for about 140 years according to the current annual consumption rate. Figure 1.6 shows estimated world reserves of tungsten in different countries [9].

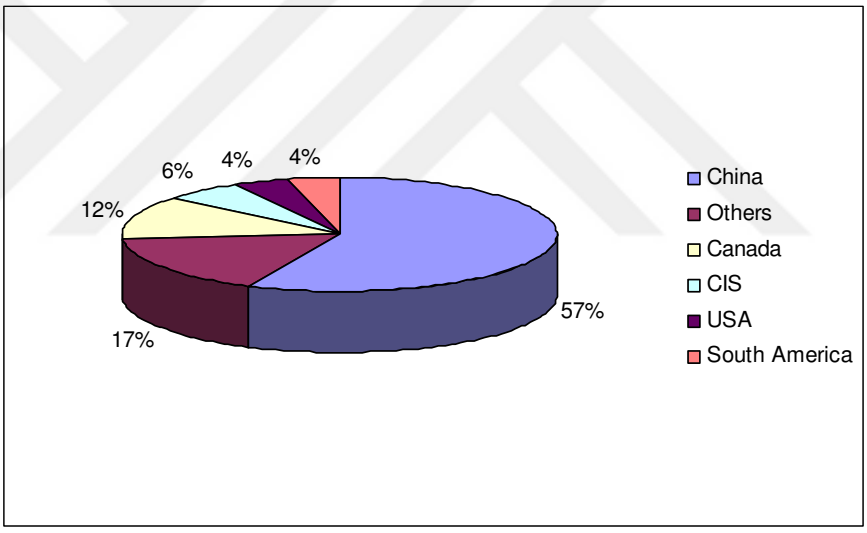


Figure 1.6: Estimated World Reserves of Tungsten in Different Countries [9] (CIS=Community of Independent States)

Türkiye's total tungsten reserves are estimated at about 15 million tonnes (≈ 0.5% WO_3) [10]. Therefore, tungsten content of these ores can be calculated as approximately 60000 tonnes, which corresponds to nearly 1% of total world reserves of tungsten.

CHAPTER 2

LITERATURE REVIEW

2.1 Industrial Production

Most of the time industrial production of tungsten starts with formation of the important intermediate product "ammoniumparatungstate" (APT, formula: $(NH_4)_{10}[H_2W_{12}O_{42}]4H_2O$). Flowsheet considerations associated with the APT production from the ore can be seen in Figure 2.1 [11]. Today's only technically important method for tungsten powder production is the hydrogen reduction of tungsten oxides at temperatures between 600 - 1100 $^{\circ}$C in a streaming hydrogen atmosphere. Therefore APT is mostly converted into tungsten oxides first and then reduced to tungsten metal (Figure 2.2) [12]. The overall reduction reaction can be given as:

$$WO_3\,(s) + 3H_2\,(g) = W\,(s) + 3H_2O\,(g)$$

As starting materials, besides the trioxide, tungsten blue oxide (WO_{3-x}) or tungstic acid (H_2WO_4) are also in use. In fact, the reduction of WO_3 to W as described by the simple equation above is in reality a rather complex process. The reduction process proceeds in distinct stages, through the formation of all stable oxides:

$$WO_3(\text{yellow}) \rightarrow WO_{2.9}(\text{blue}) \rightarrow WO_{2.72}(\text{violet}) \rightarrow WO_2(\text{brown}) \rightarrow W(\text{gray})$$

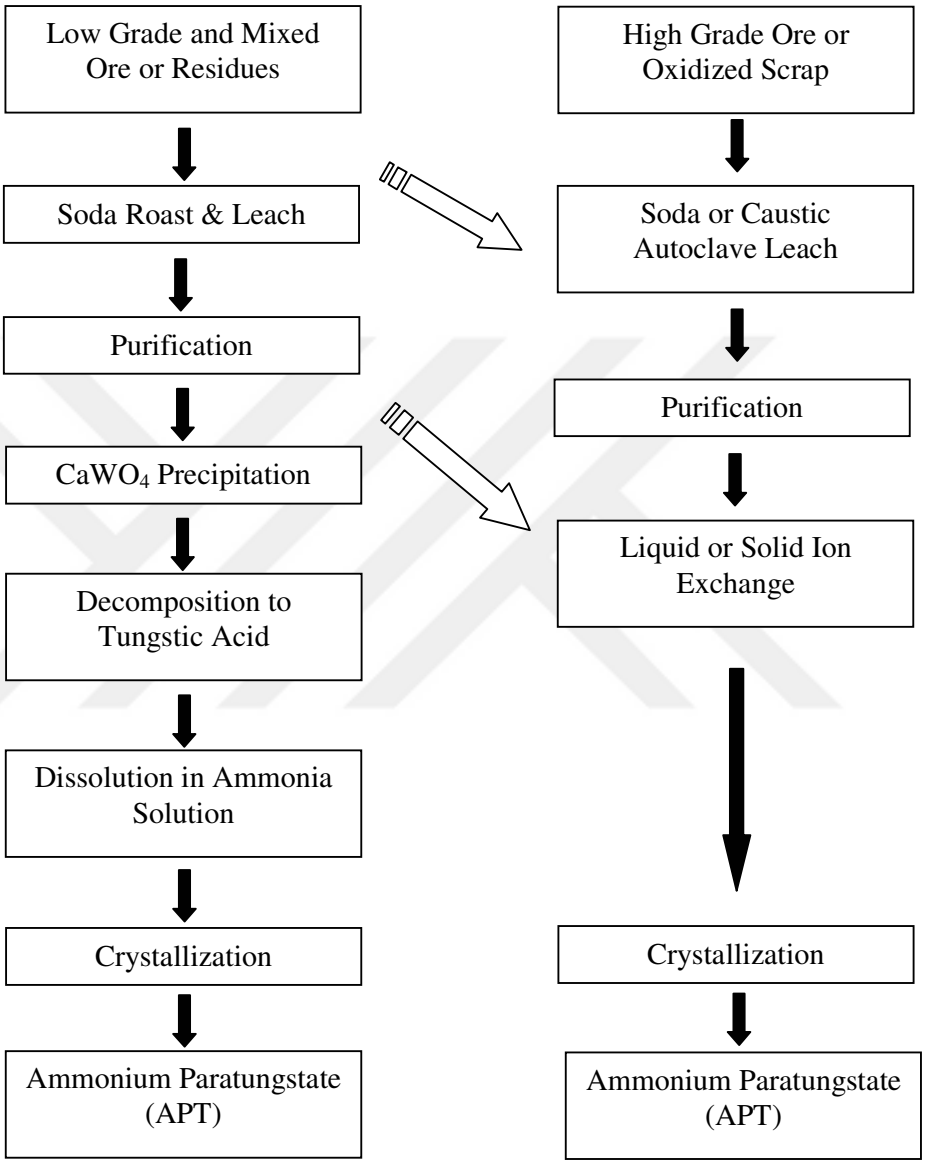


Figure 2.1: Flowsheet of APT Production from the Ore [11] (Arrows between the two columns indicate alternative roots)

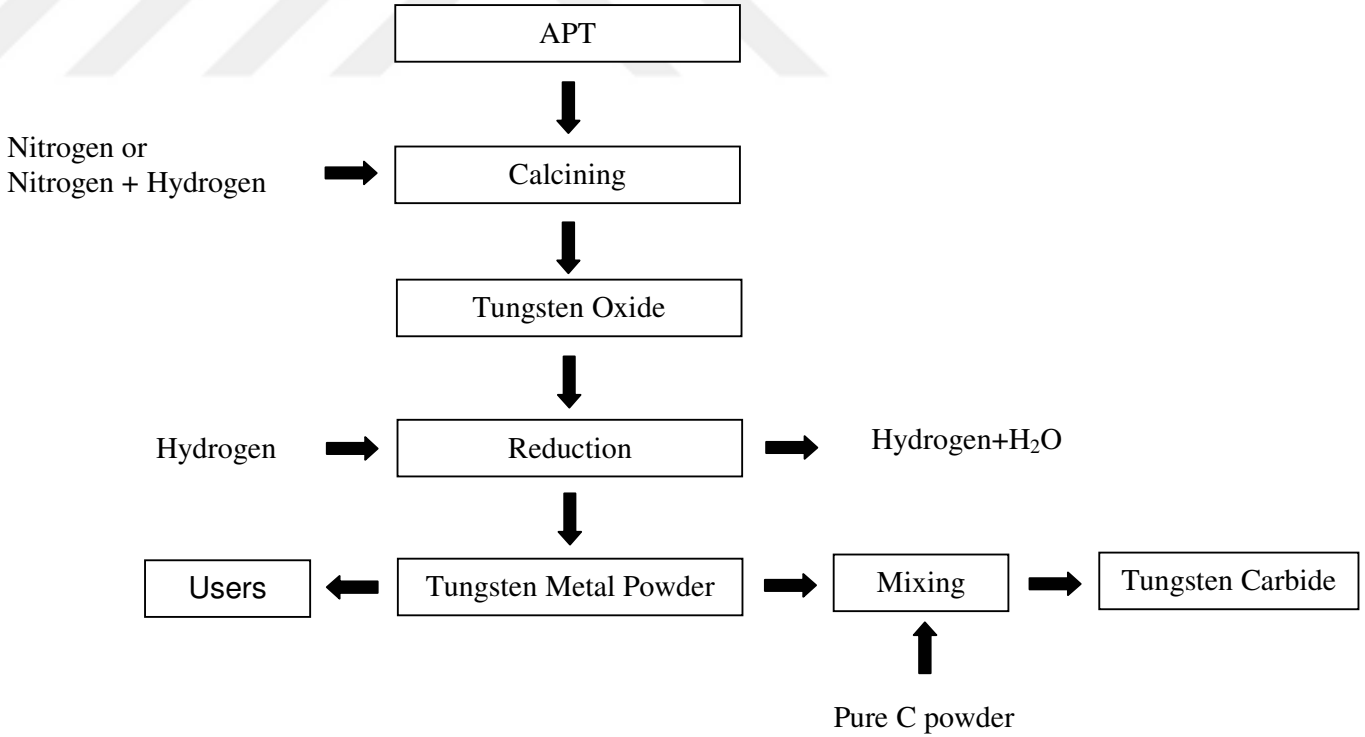


Figure 2.2: Tungsten Production from APT (Most of the metal is then used in the manufacture of tungsten carbides. [12])

The reduction process is not only a chemical conversion from oxide to metal. It is combined with a chemical vapor transport of tungsten which is responsible for the final powder characteristics. By changing the reduction parameters the powder properties like average grain size, grain size distribution, grain shape, agglomeration, etc. can be regulated within a considerable wide range and this makes the process unique in a certain sense. Besides chemical conversion and chemical vapor transport, the reduction process is a purification step, too. Trace impurities, always present in the oxide, may evaporate.

2.2 Disadvantages of the Current Process and Alternative Processes

When selecting a reducing agent for a particular compound, one of the most important requirements is a large negative Gibbs energy change for the reduction reaction. Other requirements are; high boiling point of the element, low melting point of its oxide and finally the low cost of reducing agent. At low temperatures, calcium and magnesium have the largest reducing potential but they loose effectiveness at high temperatures because of their low boiling points. Aluminum and silicon are most widely used for metallothermic reduction and the former is generally superior to the latter over the temperature range up to the boiling point of aluminum. Although carbon is a poor reducing agent at low temperatures, its reducing capability increases with temperature and it is the most widely used reducing agent especially at high temperatures. Hydrogen is also used in some cases where metallothermic and carbon reduction techniques are not suitable.

Usually, some heat must be supplied for the initiation of the reduction reaction. However, after initiation, if the reaction is highly exothermic, it may be self-sustaining; which means no further external heat supply is necessary. Reductions with calcium, magnesium and aluminum are generally sufficiently exothermic

and no further heat supply is required. On the other hand, when hydrogen, silicon or carbon is used as the reducing agent, the process is usually conducted with external heat supply.

Tungsten powder is produced by hydrogen reduction. The process has certain disadvantages:

1) There is considerably low driving force for the process at the temperatures of reduction. For a large negative Gibbs energy change (large driving force) for the reduction reaction, the line of the reductant must be far below the line of the reduced metal on the corresponding Ellingham Diagram. However, as it can be seen from Figure 2.3, H_2-H_2O line is only slightly below W-WO_3 line at the temperatures of reduction [13].

2) It is conducted with continuous external heat supply.

3) Hydrogen is a difficult gas to handle.

However, in tungsten production, the major concern is product purity because good ductility and fabricability of tungsten depend strongly on the purity of the metal. Since hydrogen is easily obtainable, it is used industrially as a reductant for tungsten oxides instead of carbon or other reducing agents.

In some cases (e.g. tungsten used as an alloy addition), the purity requirement is less stringent, and carbon may be used for the reduction process but the resultant powder usually contains some silicon, iron, carbon, sulphur, and phosphorus impurities.

Metallothermic reduction has also been used in small scale or for some special purposes, but after reduction, a refining process such as electro-refining is necessary. Another drawback of metallothermic reduction is that the final shape of the product is not fine powder. This leads to difficulties during consolidation in subsequent powder metallurgy processes.

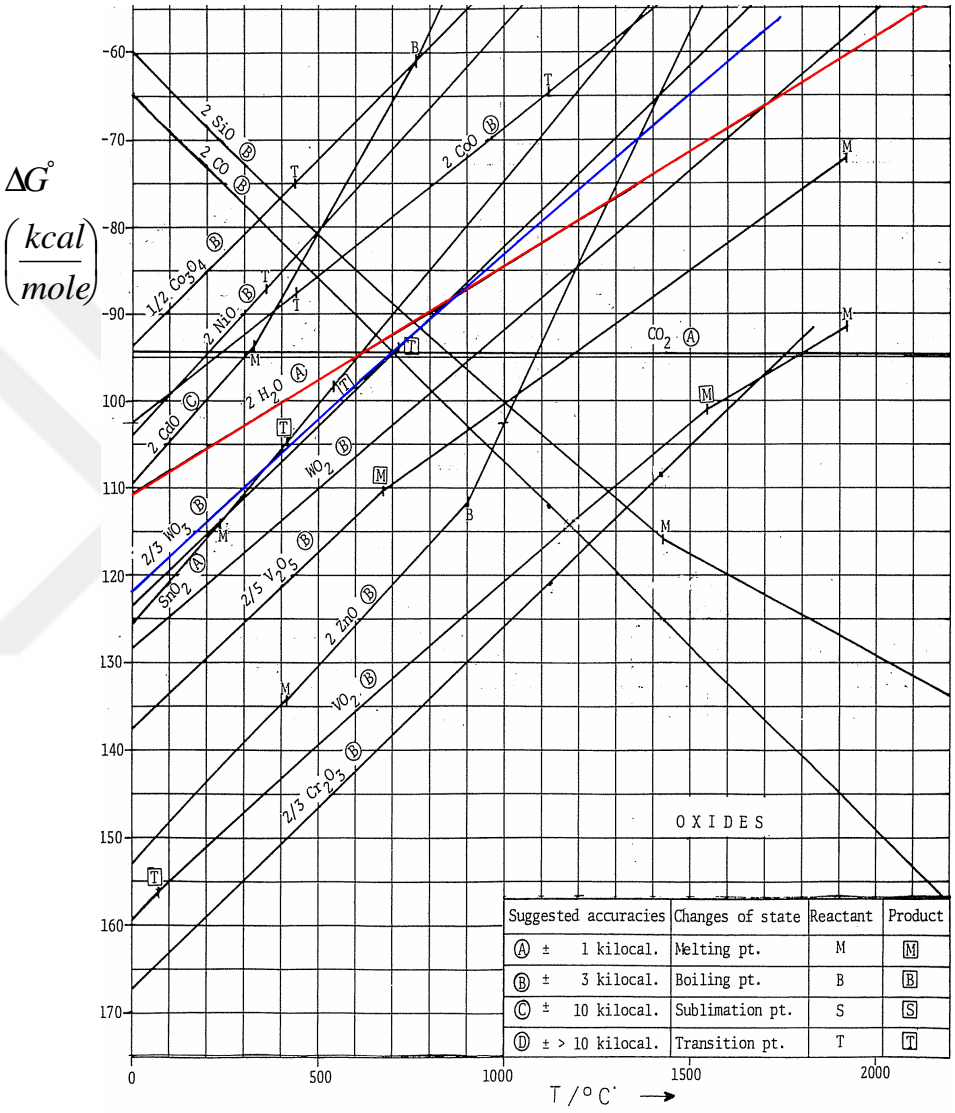


Figure 2.3: Ellingham Diagram for Metal-Metal Oxide Systems (W-WO_3 line is in blue and H_2-H_2O line is in red, reproduced from [13].)

There have also been some studies to produce high purity tungsten metal by the electrolysis of various molten salts, but none have been successful on a commercial scale. In general molten salt electrolysis for electrodeposition of metals have some problems in common, such as; dendritic deposition, consequent oxygen contamination of products upon exposure to air, and redox cycling reactions of multi-valent metal ions that become even more active in molten salts because of high temperatures. For tungsten electrowinning, the most important problem is the large particle size of the electrowon tungsten. This leads to a relatively porous product when consolidated by the classical pressing and sintering techniques.

2.3 FFC Cambridge Process

Molten salt processing is used in metal extraction for more than a century. Metals having very stable compounds can not be produced by gas-based pyro-reduction, metallothermic reduction, hydrometallurgical methods or aqueous electrochemical techniques. In these cases, where production by other routes is not feasible due to thermodynamic, kinetic or economical constraints, the option is limited to electrowon the metal by the electrolysis of various molten salts. However fused salt electrolysis is satisfactory only for low melting point metals which are deposited in the liquid state. High melting point metals can be electrowon in the solid state because the reduction temperature is less than the melting point. But this results in dendritic deposition which is prone to oxidation.

The classical molten salt electrolysis involves dissolution of the starting material, containing the metal to be electrowon, in the electrolyte. A subsequent electrowinning of the metal from the solution takes place by direct current reduction. Therefore, there had been some attempts to produce metals from their oxides by dissolving the metal oxide in fluoride melts because fluorides are

regarded to be better at dissolving oxides than chlorides. However, most of the time these studies failed to develop a commercial large scale production because fluorides usually melt at higher temperatures and they are far more corrosive. Until quite recently, the only molten salt process involving electrochemical reduction of oxides industrially was the Hall-Heroult process for the electrowinning of aluminum from alumina.

In 1997, a novel process has been reported for the production of metals from their oxides by electrolysis in fused salts. The process is called as FFC (Fray-Farthing-Chen) Cambridge process and it is claimed to be more suitable for electroreduction of the high-melting transition metal oxides and actinides.

In metal-oxygen systems oxygen can take two forms; chemically bound oxygen as oxide or dissolved oxygen as solid solution. Calcium oxide is the most stable metal oxide, therefore calcium is used as a very effective deoxidant in metal-oxygen systems. The general form of the reaction can be written as:

M(O) + Ca = M + CaO

Therefore, equilibrium oxygen content of the metal can be calculated from:

$$[O]=\left(\frac{a_{CaO}}{a_{Ca}}\right)\left(\frac{1}{f_O}\right)\exp\left(\frac{\Delta G^\circ}{RT}\right)$$

ΔG° = Standard free energy change of the reaction

f_O = Activity coefficient of oxygen in the metal

a_{CaO} = Activity of calcium oxide referred to pure state as the standard state

a_{Ca} = Activity of calcium referred to pure state as the standard state

From the above equation, it is clear that for a given system with constant f_O, the lower the $\frac{a_{CaO}}{a_{Ca}}$ ratio gets, the lower the oxygen concentration in the metal will be. However, with time CaO formed, makes a thick coating around the metal surface and inhibits further reduction by interrupting the contact between the metal and calcium. Therefore, $\frac{a_{CaO}}{a_{Ca}}$ ratio becomes quite high at the reaction interface. This problem can be overcome by conducting the reduction in a medium in which both Ca and CaO can dissolve. At this point molten salts are incorporated into the process because alkaline earth chlorides have very high solubility for their respective oxides. Therefore if the process is conducted in the molten medium ($CaCl_2$ in the case of Ca reduction), the CaO dissolves in the molten salt flux and no longer acts as barrier. Finally electrochemistry is incorporated into the process because the process will require continuous supply of Ca on to the metal and removal of CaO from the melt in order to keep $\frac{a_{CaO}}{a_{Ca}}$ ratio low at the reaction interface.

For the first time, Ward and Hoar [14] had removed oxygen, sulphur, selenium and tellurium from molten copper by electrochemical technique. Graphite was used as the anode and the electrolyte was $BaCl_2$. A potential, which was above the decomposition potential of $BaCl_2$, was applied to remove the non-metallic impurities. The overall cell reaction was assumed to be:

$BaCl_2 = Ba + Cl_2$

Elemental Ba produced at the cathode surface was considered to react with impure copper according to the below reaction:

$Cu_2X + Ba = 2Cu + BaX$

where X is O, S, Se or Te.

Similar to above application, Okabe et al have developed many techniques for removal of oxygen from titanium in calcium saturated calcium chloride melts [15-17]. They could achieve the lowest oxygen impurity level of about 10 ppm, when the reductant Ca metal is generated in-situ by electrolysis of calcium chloride. The calcium metal produced by the electrolysis reacts with oxygen in titanium to give calcium oxide. This CaO dissolves in calcium chloride, and is electrolyzed to regenerate Ca for further reduction. The cell arrangements in both cathodic refining techniques ([14], [15-17]) were identical and given in Figure 2.4.

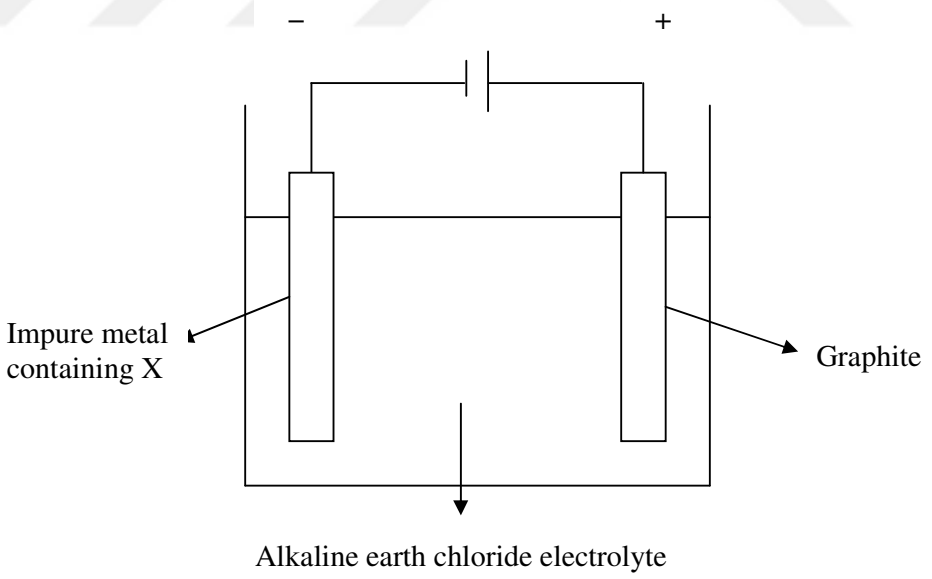


Figure 2.4: Cell Arrangement of Cathodic Refining Technique

Chen and Fray have also done similar experiments on cathodic refining of copper [18] and titanium [19]. They applied potentials which were lower than the decomposition potential of the salts, but they could still achieve deoxygenation. As a result of these observations, they concluded that, electrolysis of the salt to produce Ca or Ba and their chemical reaction with the oxygen (or the impurity element) were not necessary for the deoxygenation.

Removal of oxygen (or the impurity element) takes place via its cathodic ionization and following discharge at the anode.

$X + 2e^- = X^{2-}$ (cathode reaction)
$X^{2-} = X + 2e^-$ (anode reaction)

FFC Cambridge Process is a high temperature electrolysis process in molten salts to obtain metals or alloys from the starting material as oxide, sulphide, carbide or nitride. However almost all the work so far has been for metal production from their oxides and especially titanium production from titanium dioxide. The cell arrangement, given in Figure 2.5, is very similar to the cathodic refining technique discussed above. Electrolysis is conducted between the graphite rod anode and the metal oxide cathode in the molten salt media containing $CaCl_2$ as the major component. By the application of a voltage, which is lower than the decomposition potential of the molten salt but higher than the decomposition potential of the metal oxide, the oxygen ions leave the metal oxide cathode and move towards the graphite rod anode, forming CO and/or CO_2 depending on the temperature. The reactions are:

$M_xO_y + 2ye^- = xM + yO^{2-}$ (Cathodic reaction)

$yO^{2-} + yC = yCO + 2ye^-$ (Anodic reaction)

$M_xO_y + yC = xM + yCO$ (Overall reaction)

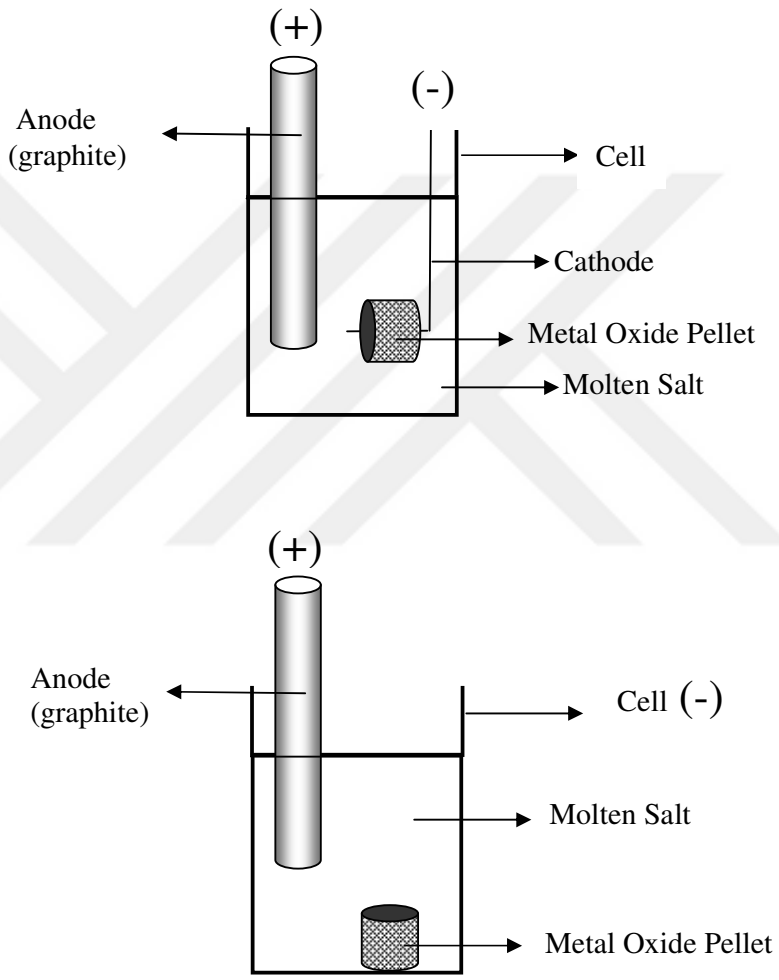


Figure 2.5: Two different cell arrangements of FFC Cambridge process. In the upper one, a wire is used as the current collector. In the lower one, crucible itself is made the current collector.

In the case of an inert anode, the anode and the overall reactions will be:

$yO^{2-} = y/2\ O_2 + 2ye^-$ (Anodic reaction)

$M_xO_y = xM + y/2\ O_2$ (Overall Reaction)

2.4 The Objective of This Research

As it was mentioned previously, the current process, which is used to produce tungsten, has many disadvantages. However, extensive research in recent years has failed to develop any essentially new method of large-scale production. By the FFC Cambridge process discussed in section 2.3, Ti [20], Cr [21], Si [22], Cu [23], Al, B, Fe, V, Nb, U, Nd, Zr, Hf, Ce, and Ni [24-26] have already been reduced in laboratory experiments. In addition, K. Dring et al have recently reported that Ti–W alloys were produced via electrochemical reduction of TiO_2–WO_3 mixed oxide preforms in molten calcium chloride electrolyte at 900°C [27]. In the light of above findings, direct electrochemical production of tungsten with an electrolysis setup, which is in some ways similar to FFC Cambridge process, was investigated. Feasibility of electroreduction of tungsten compounds may lead to the development of alternative tungsten production methods.

CHAPTER 3

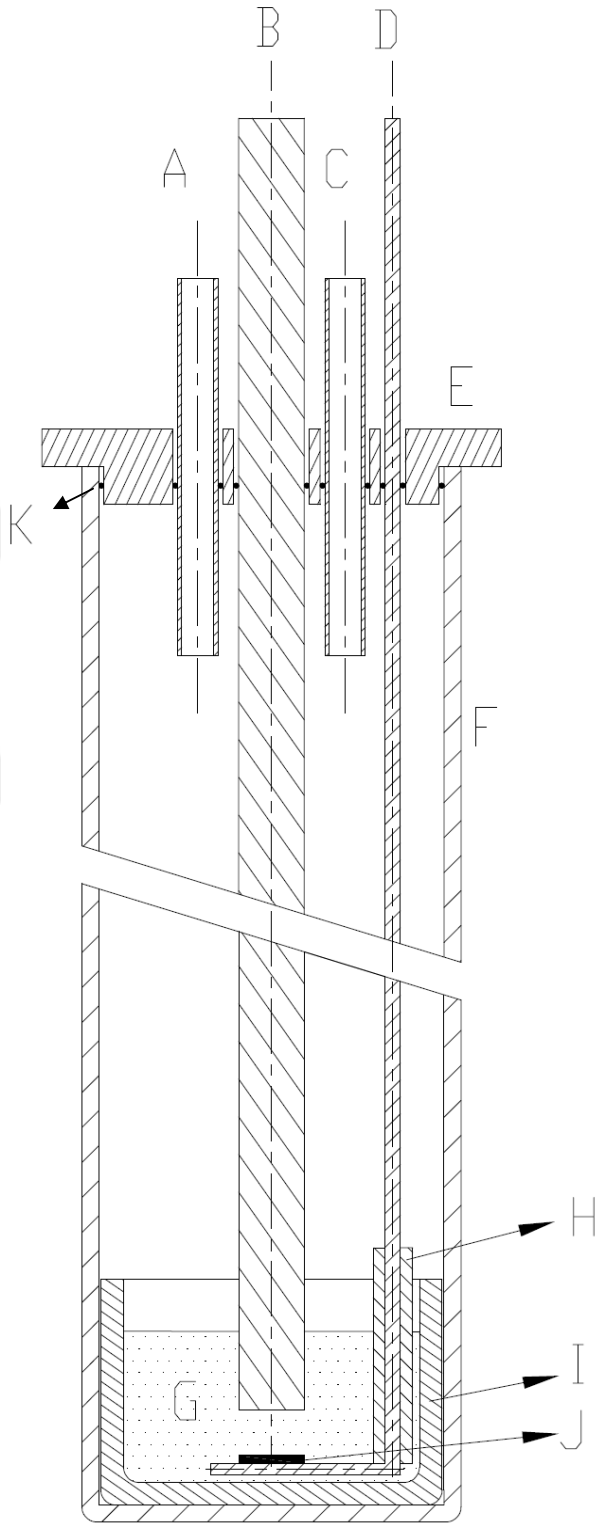
EXPERIMENTAL

Only the first experiment was conducted with tungsten trioxide (WO_3) as the starting material and pure calcium chloride ($CaCl_2$) as the electrolyte. Details of this experiment will be given in section 4.1. All the other experiments were conducted with $CaWO_4$ as the starting material and eutectic sodium chloride (NaCl) – $CaCl_2$ salt mixture as the electrolyte. Therefore all the sections of this chapter will refer to the latter experiments.

3.1 Experimental Setup

3.1.1 Cell Assembly

The schematic drawing of the cell assembly is shown in Figure 3.1. A calcium tungstate ($CaWO_4$) pellet forming the cathode of the cell was placed into a spoon (made up of stainless steel), which was welded to the end of a stainless steel wire current collector. This wire was covered by an alumina insulator near the bottom of the cell to prevent any short circuit problem during the experiment. A graphite rod (A10134, Alfa Aesar) was used as the anode material. An alumina crucible (10 cm long, 4 cm outside diameter), positioned into a quartz vessel (60 cm long, 5 cm inside diameter), was used to hold the electrolytic cell. The cell vessel was covered at the top by a Teflon lid, which had four holes on it. Connections to cell were made through the Teflon lid by employing rubber o-rings to each hole. By this way, the stainless steel cathode connection and the graphite rod anode were vertically movable without gas leak. The hole at the centre (13 mm diameter)



A: Argon Inlet

B: Graphite Anode

C: Gas Exit

D: Stainless Steel Cathode Connection

E: Teflon Lid

F: Quartz Cell Vessel

G: Molten Salt ($CaCl_2$-NaCl)

H: Alumina insulator for cathode lead

I: Alumina crucible

J: $CaWO_4$ cathode

K: O-rings

Figure 3.1: Schematic Drawing of the Cell Assembly

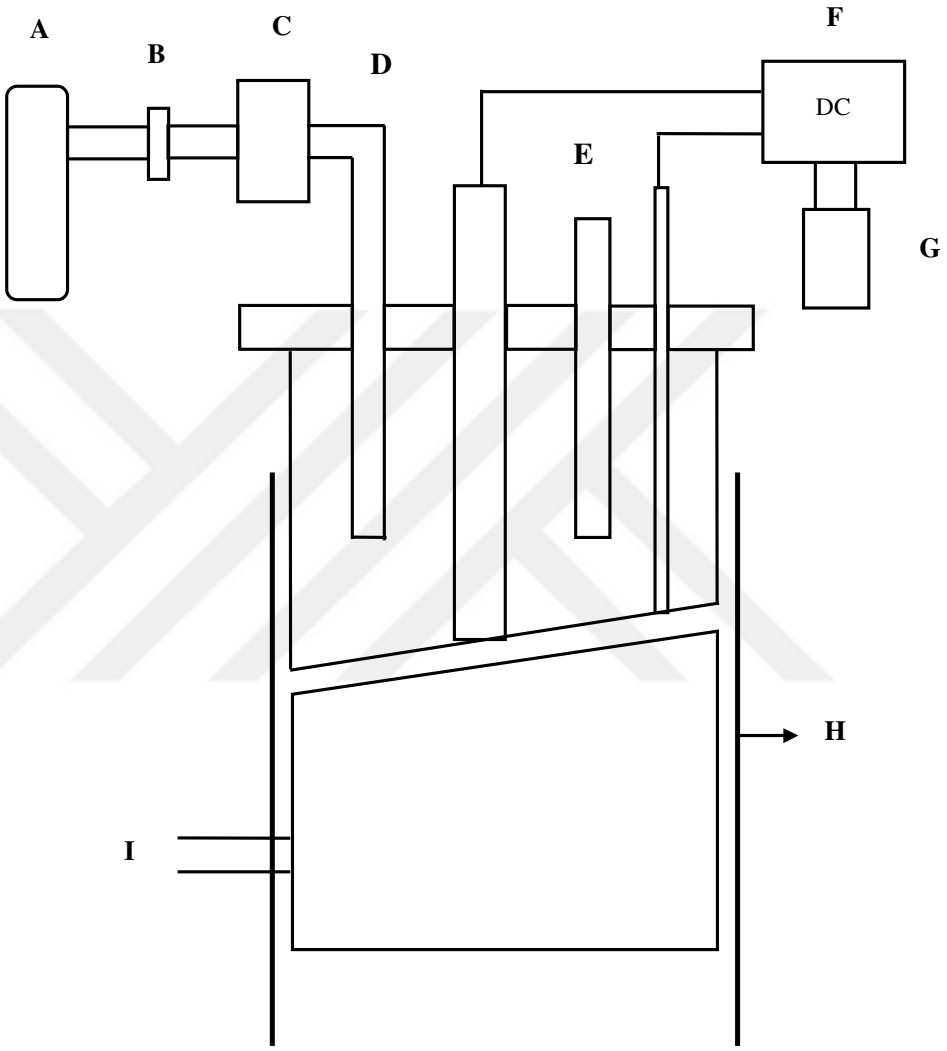
was used to install the graphite rod anode and the other three holes were located around this central hole. The holes with 8 mm diameters were used for argon inlet and gas outlet. And the remaining hole (3 mm) was used to place the cathode assembly.

Quartz cell vessel was placed into a vertical tube furnace to a depth of about 40 cm. Upper portion of the cell vessel remained outside the vertical tube furnace during the electrolysis. Therefore, the necessary electrode movements were made possible by electrode leads extended from the top of the cell. Furthermore, electrical and gas connections at a temperature close to room temperature enabled an easier operation.

Quartz was used as the vessel material to withstand the high operating temperatures as well as the high temperature differences along the height of the cell vessel. Furthermore, quartz is chemically inert to many species which makes it very suitable as a vessel material.

3.1.2 Auxiliary Apparatus

A schematic drawing of the auxiliary apparatus is shown in Figure 3.2. The power for electrolysis was provided by a programmable GW Instek PPS-3635 DC power supply. Corresponding current values and potential differences between the electrodes were read from the power supply and verified by a Goldstar DM-341 type multimeter. In the experiments, variations of current values at an applied constant potential, and/or potential differences at an applied constant current value were recorded as a function of time. A Lindberg LHTF3226 Kanthal wire wound vertical tube furnace was used to accommodate the cell assembly. The furnace could be programmed with the desired ramp/dwell combinations. Desired cell temperature was obtained by a thermocouple placed just outside the cell vessel. Measurements of temperature profile of the furnace indicated close agreement of hot zone temperature with the above thermocouple. An argon gas flow of 100 ml/minute was used to provide



A: Argon Gas
B: Flowmeter
C: Drying Column
D: Argon Inlet
E: Gas Outlet
F: DC Power Supply
G: Multimeter
H: Vertical Tube Furnace
I: Thermocouple

Figure 3.2: Schematic Drawing of the Auxiliary Apparatus

an inert atmosphere in the cell vessel and also argon was used as a carrier gas to take gaseous electrolysis products out of the cell vessel. It was passed through drying columns before introduced to the cell vessel from the gas inlet part. A photograph of the experimental setup is given in Figure 3.3.



Figure 3.3: A view of the experimental setup

3.2 Experimental Procedure

3.2.1 Cell Feed Preparation

A commercially available tungsten trioxide (WO_3) powder (95410, Fluka) was selected as one of the starting materials. It is mixed with an equimolar calcium oxide (CaO) powder in a mixer for 60 minutes. Then this powder mixture was

heated to 1200°C and held for 360 minutes to convert the whole powder into $CaWO_4$ according to the reaction:

$CaO\ (s) + WO_3\ (s) = CaWO_4\ (s)$

Completion of conversion was tested by X-ray diffraction analysis and the result of one of the tests is given in Figure 3.4.

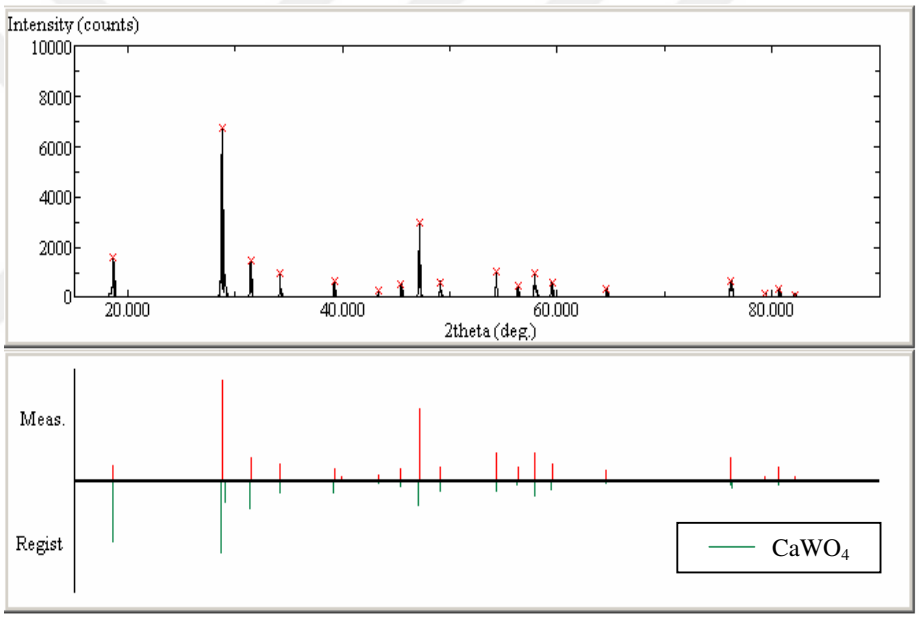


Figure 3.4: X-ray Diffraction Spectrum of the Sample after Complete Conversion to $CaWO_4$

This $CaWO_4$ powder was treated with a binder (polyvinyl alcohol (PVA) or polyethylene glycol (PEG)) depending on the subsequent process. If the pellet was to be sintered after pressing, PVA was used as the binder. The amount of it was 2% by mass of $CaWO_4$, and the components were mixed for 40 minutes. The powder was dried in air at room temperature for 24 hours and then passed

through a sieve to prevent any agglomeration. After that, it was pressed in the form of a pellet of weight 2.5 grams, diameter 1.5 cm and height 0.3 cm. The resulting pellet was sintered at 1200°C for 120 minutes. However, if the only mechanically pressed pellet was to be used directly in the experiment, PEG was used as the binder, and the amount was 3% by mass of $CaWO_4$. Similarly the components were mixed for 40 minutes and then left to dry in air at room temperature for 24 hours. Following the sieving stage, PEG was removed by holding the pellet at 600°C for 150 minutes (This temperature is too low for the $CaWO_4$ powder to sinter). Then, the powder mixture was pressed in the form of a pellet of the same size as stated above. In both cases, the pellets were pressed under 2-3 tonnes load. The flowchart of pellet preparation is given in Figure 3.5.

$CaCl_2$ (12095, Riedel-de-Haën) – NaCl (13423, Riedel-de-Haën) salt mixture at eutectic composition was used as the electrolyte. Both salts were dried prior to each experiment without producing oxides and hydroxides of the salts.

It requires close experimental attention to obtain anhydrous, oxide free $CaCl_2$. Therefore, it was first heated to 110°C at 10°C/min and held for three hours. Then the temperature was ramped to 400°C at 1°C/min and held for 24 hours. All the process was conducted under vacuum and by this way, physically and chemically bound moisture in $CaCl_2$ could be removed. The phase diagram with possible phase boundaries, shown by the dashed lines, for $CaCl_2$-H_2O system at low HCl pressure (10^{-3} atm), is shown in Figure 3.6 [28]. With reference to figure 3.6, it can be concluded that above procedure, involving dehydration at low pressures, could yield oxide free anhydrous $CaCl_2$.

On the other hand, NaCl was just heated to 110°C and held at this temperature for 24 hours. The phase boundary between NaCl and NaOH is shown in Figure 3.7 [28]. As it is apparent from the figure, unlike $CaCl_2$, the equilibrium partial pressure of water to form NaOH is extremely high.

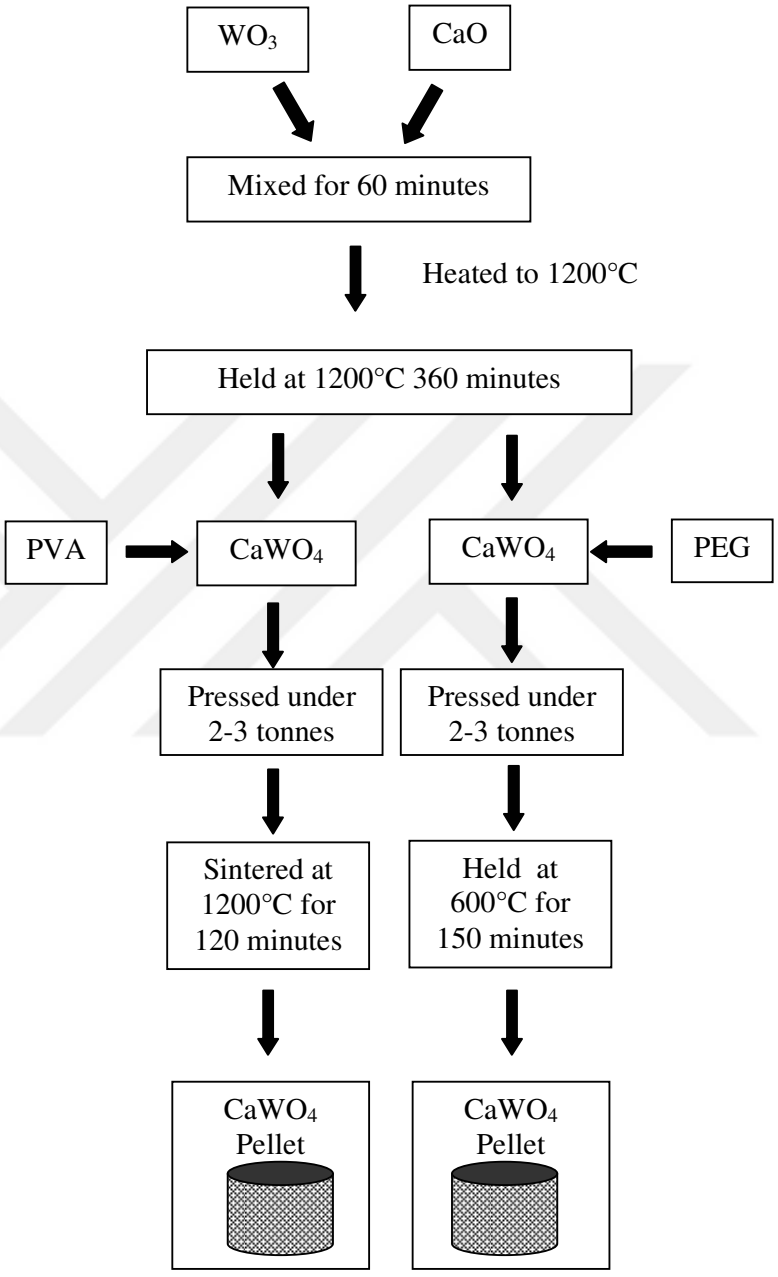


Figure 3.5: Flowchart of Pellet Preparation Procedure

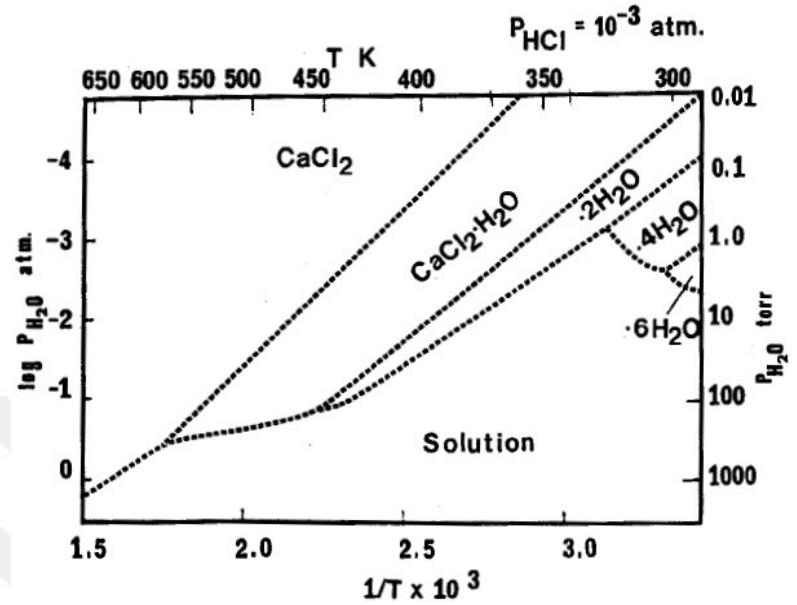


Figure 3.6: Approximate equilibrium diagram for the $CaCl_2$-H_2O system at an HCl partial pressure of 10^{-3} atm. showing possible phase boundaries between the hydrates and the solution. The $Ca(OH)_2$ is off scale at the lower left. Reproduced from [28].

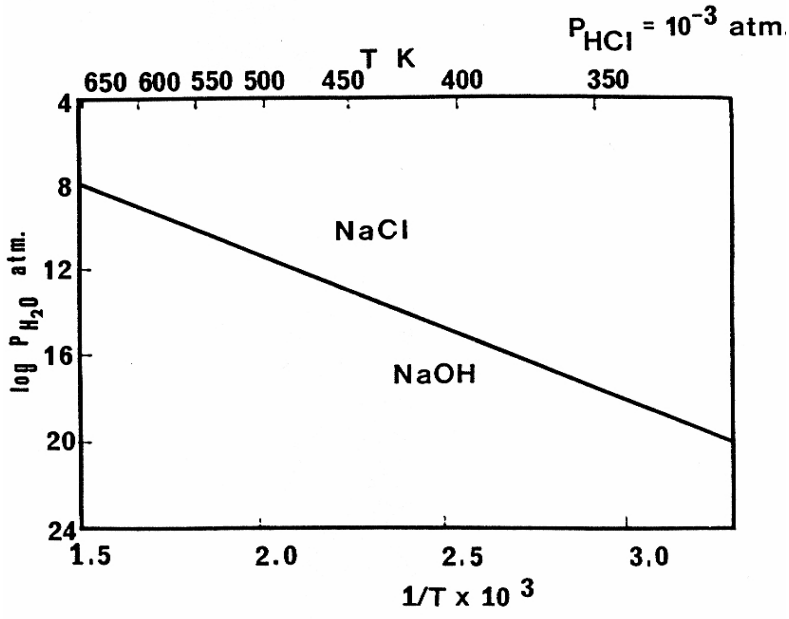


Figure 3.7: Equilibrium diagram for the NaCl-H_2O system at an HCl partial pressure of 10^{-3} atm. Reproduced from [28].

3.2.2 Cell Operation:

The cell containing approximately 100 grams of electrolyte (69.3 gm $CaCl_2$, 33.7 gm NaCl) was placed into the vessel. The cover accommodating electrode assembly etc. was then placed over the vessel (Figure 3.1). This vessel is then placed into the vertical tube furnace as shown in Figure 3.2. The heating process was started after all the connections to the auxiliary apparatus were completed. Any residual moisture of $CaCl_2$ was removed during heating by applying slow heating rates and long dwell times. Temperature was first ramped to 400°C at 10°C/min (thermal pre-drying had been done at this temperature before, see section 3.2.1) and held at this temperature for 10 to 15 minutes. Then the temperature was ramped to the target temperature of 600°C at 2°C/min. The whole heating process and the electrolysis experiment were conducted under continuous flow of argon gas.

The actual electrochemical reduction experiments were carried out as follows: As it can be seen from Figure 3.8 [29], the electrolyte was in molten state when the temperature reached to 600°C. The electrodes were lowered and immersed into the electrolyte. Sufficient time was given for temperature to stabilize and concentration to homogenize as a result of mixing action of electrodes. Then the electrodes were clamped to the rectifier (DC power supply) leads.

In the experiments, applied potentials did not exceed 3.4 volts. These voltages were lower than decomposition potentials of $CaCl_2$ and NaCl ($E^{\circ}_{CaCl2} = -3.4$ V, $E^{\circ}_{NaCl} = -3.37$ V) when the overvoltages and the voltage drops along the electrode leads are taken into account. In order to determine voltage drops along electrode leads, measurements were done by short-circuiting the electrodes in a molten Pb pool. Currents, within the range of values measured during experiments, were applied. Voltage drops ($E_{electrical\ connections}$) as a function of applied currents (I) were obtained. The results are given in Figure 3.9.

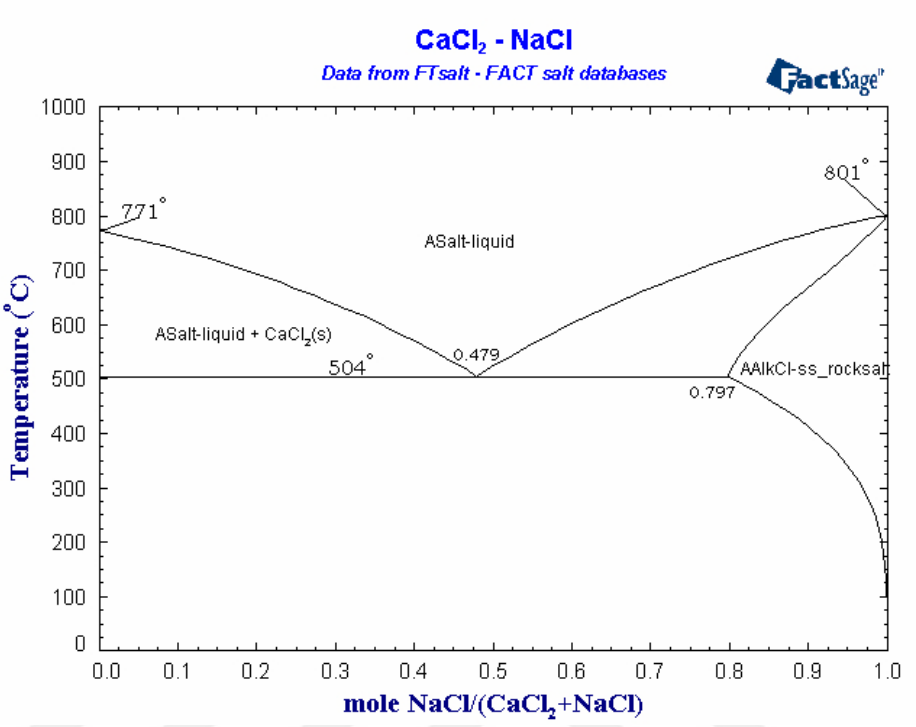


Figure 3.8: Phase diagram of $CaCl_2$-NaCl system (Reproduced from [29])

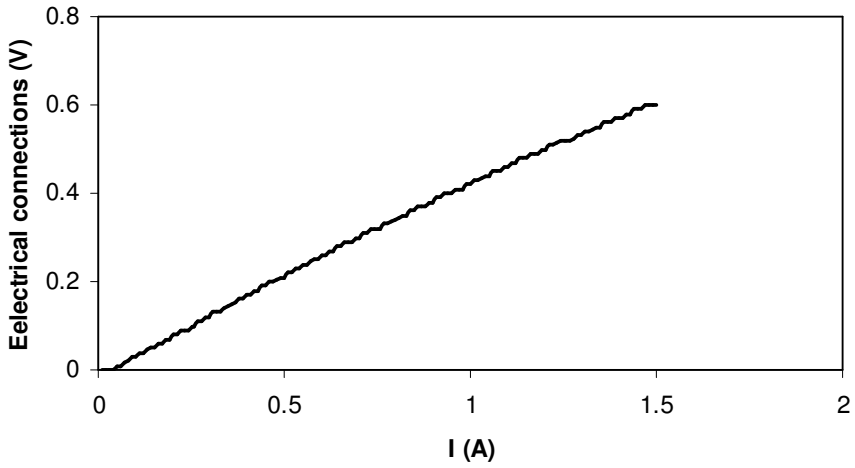


Figure 3.9: Recorded voltage values ($E_{electrical\ connections}$) as a function of applied current (I), obtained by short-circuiting the electrodes in a molten Pb pool at 600°C.

These values were used to eliminate voltage drops along the electrode leads from the measured cell voltages to obtain net cell voltages.

At the end of each experiment, cell vessel was flushed with argon to remove gaseous electrolysis products. The current was switched off after flushing period and the electrodes were removed from the molten salt mixture. Finally, the furnace power was turned off and the cell vessel was left to cool with the argon flow being maintained.

After cooling, the cathode was taken from the cell and washed with tap water in a glass vessel to remove the solidified salt around the reduced specimen. Then the sample was filtered and dried. Chemical compositions of the reduced samples were investigated by means of energy-dispersive X-ray diffraction analysis.

Some of the samples were held in a 0.2 M hydrochloric acid (HCl) solution to remove calcium oxide (CaO) and/or calcium hydroxide ($Ca(OH)_2$), that were found to be present in significant amounts at the cathode. It was observed that, tungsten was sufficiently inert under these conditions, whereas CaO and/or $Ca(OH)_2$ could easily and completely be removed.

CHAPTER 4

RESULTS AND DISCUSSION

4.1 Electrolysis of Tungsten Trioxide (WO_3)

As it was stated in section 2.4, K. Dring et al have recently reported that Ti–W alloys were produced via electrochemical reduction of TiO_2–WO_3 mixed oxide preforms in molten calcium chloride electrolyte at 900°C [27]. Therefore, in the first experiment, tungsten trioxide (WO_3) was used as the cathode material and the electrolyte was pure calcium chloride. The temperature was 900°C which was consistent with the above study. Upon immersing the electrodes into the molten salt, white fumes were observed. However, the experiment was not interrupted and carried until the end. These fumes were soon deposited to the cooler parts of the quartz cell vessel as yellow powders. After the experiment, it was realized that the pellet was distorted but it was still on the stainless steel spoon cathode. It was washed with water and then filtered and dried. Together with the yellow powder scraped from the cell vessel, a sample from the cathode was subjected to X-ray diffraction analysis for characterization.

X-ray diffraction spectra of the deposited yellow powder and the sample taken from the cathode are given in Figure 4.1 and Figure 4.2 respectively. As it can be seen from Figure 4.1, deposited yellow powder was mainly tungsten oxychloride (WO_2Cl_2) phase. This result indicates that formation of gaseous WO_2Cl_2 takes place inside the cell vessel as a result of the following chemical reaction:

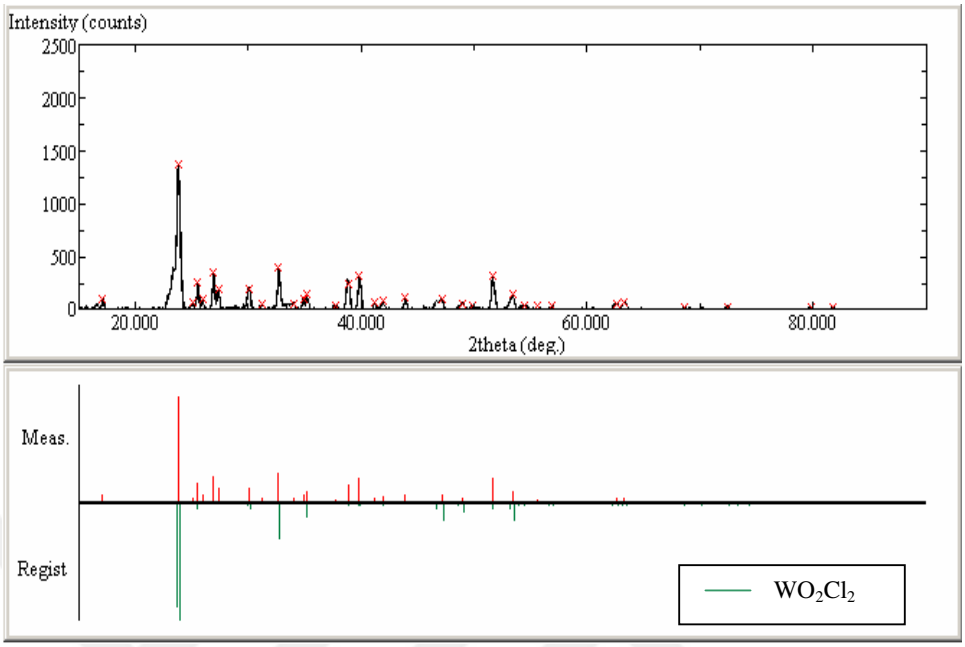


Figure 4.1: X-ray diffraction spectrum of the deposited yellow powder. The major phase is WO_2Cl_2.

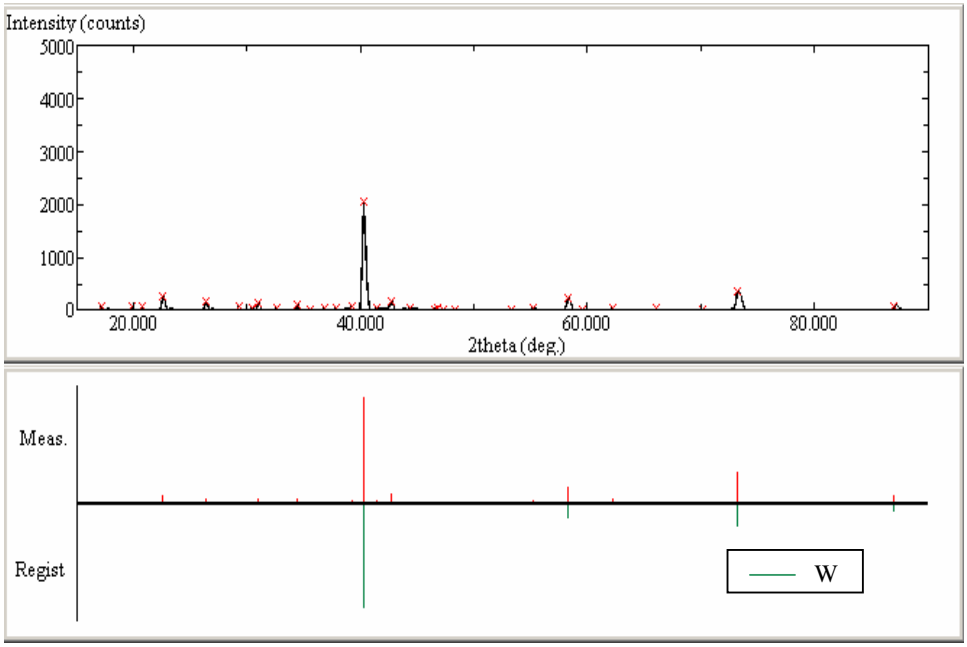


Figure 4.2: X-ray diffraction spectrum of the sample taken from the cathode. The major phase is tungsten.

$2WO_3\,(s) + CaCl_2\,(l) = CaWO_4\,(s) + WO_2Cl_2\,(g)$

According to the reaction, nearly 50% of the starting tungsten was lost, when 2.5 grams of tungsten trioxide was added to 100 grams of calcium chloride as was the case in the present experiment. The output of the F*A*C*T (Facility for the Analysis of Chemical Thermodynamics) program, which does thermodynamical calculations, for the given conditions is shown in Figure 4.3 [30]. The composition of the product phases, when WO_3 and $CaCl_2$ with given amounts were equilibrated, was calculated by Gibbs free energy minimization. Therefore tungsten trioxide can not be reduced electrochemically at high temperatures without loss, because it reacts with calcium chloride by liberating volatile tungsten oxychloride.

Examination of the X-ray diffraction spectrum in Figure 4.2 indicates the presence of metallic tungsten in the electrochemically reduced sample in spite of the above reaction. Therefore it was concluded that, in the experiment, tungsten was produced from the electroreduction of $CaWO_4$ instead of WO_3. In other words, $CaWO_4$, which was produced according to the above reaction, could be reduced to tungsten by electrolysis.

Experiment involving the use of WO_3 was performed at two different stages. In the first 35 minutes, corresponding voltage values ($E_{observed}$) were recorded as a function of time at an applied constant current value. As it is seen from Figure 4.4, voltage values increased up to 3.4 volts when 2.5 amperes of constant current was applied. To stop further increase in cell voltage, potential between the electrodes was set constant at 3.4 volts and current values were recorded until the end of the experiment. Above value was selected for applied voltage to eliminate any decomposition of $CaCl_2$ ($E^{\circ}_{CaCl_2} = -3.2$ V at 900°C). Figure 4.5 shows the variation of current with time when applied potential was 3.4 volts. As it can be seen from this figure, most of the tungsten compound used in electroreduction was reduced within the initial 50 minutes.

FACT Format

T = 1173 K, P = 1 atm, (gram) 2.5 WO3 + 100 CaCl2 =

0.51895 litre (99.999 vol% WO2Cl2
+ 0.36558E-03 vol% CaCl2
+ 0.23359E-03 vol% Cl
+ 0.79773E-04 vol% WCl4
+ 0.43944E-04 vol% Cl2
+ 0.40481E-04 vol% WCl2
+ 0.40935E-06 vol% OWCl4
+ 0.72924E-08 vol% WCl5
+ .....
(1173.00 K, 1 atm, gas_ideal)

+ 99.402 gram CaCl2
(1173.00 K, 1 atm, L1, a= 1.0000)

+ 1.5523 gram (CaO)(WO3)_scheelite
(1173.00 K, 1 atm, S1, a= 1.0000)

+ 0.00000 gram WO3
(1173.00 K, 1 atm, S2, a=0.58484E-01)

Figure 4.3: Result of thermodynamic equilibrium calculations by F*A*C*T program under the conditions of the experimental work [30].

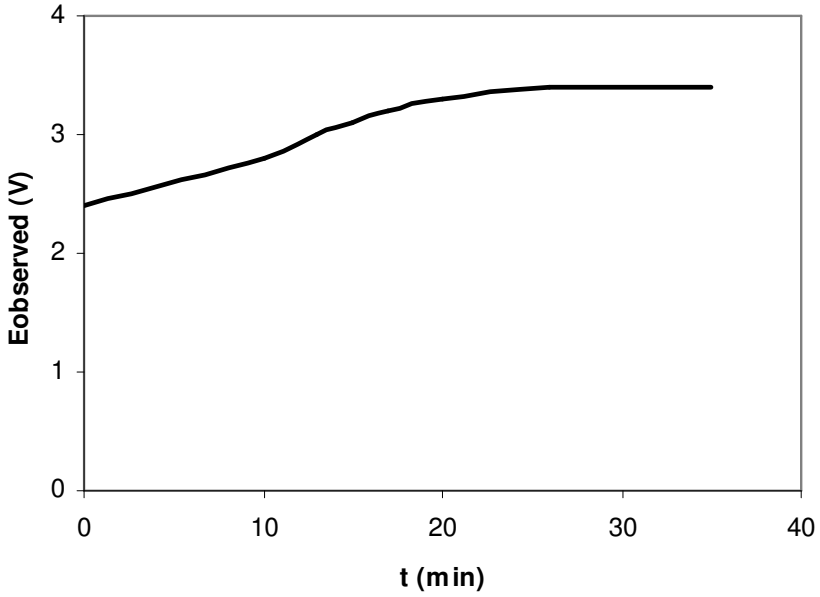


Figure 4.4: Voltage versus Time Graph at a Constant Applied Current Value of 2.5 A

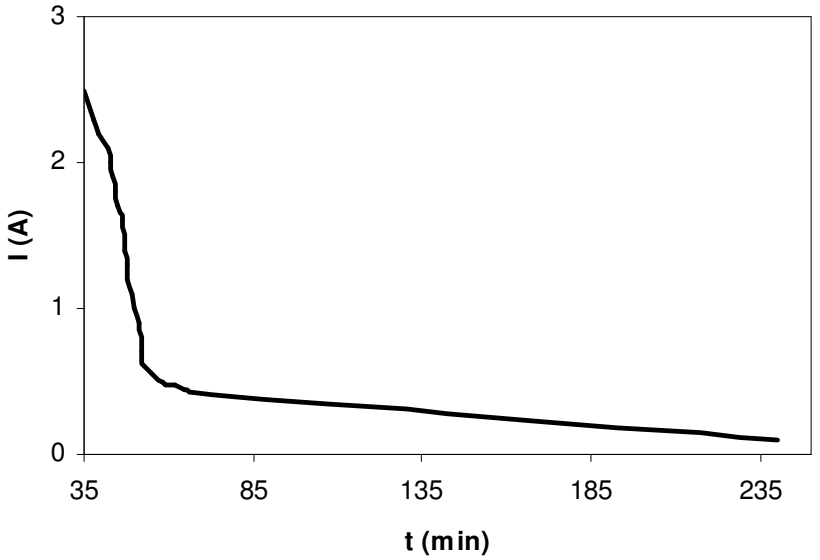


Figure 4.5:Current versus Time Graph at a Constant Potential Value of 3.4 V

In order to test the conclusions that were drawn from the experiment with the starting material as WO_3, further studies were done by using $CaWO_4$ as the starting material for the electrolysis.

4.2 Electrolysis of Calcium Tungstate ($CaWO_4$)

4.2.1 Experimental Procedure and Results:

In order to stop the reaction between WO_3 and $CaCl_2$, $CaWO_4$ was formed before the experiment, with the addition of CaO to WO_3 according to the below reaction. By this way, reaction between WO_3 and $CaCl_2$ was prevented and tungsten losses as WO_2Cl_2 were inhibited. (See section 3.2.1 for the details of pellet preparation)

$$CaO\ (s) + WO_3\ (s) = CaWO_4\ (s) \qquad \Delta G^\circ = -160381\ J/mole\ at\ 1200^\circ C$$

Above reaction has sufficiently large driving force for $CaWO_4$ formation. Completion of formation was evident from X-ray diffraction results given in Figure 3.4. However, $CaWO_4$ has significant solubility in calcium chloride at high temperatures (Figure 4.6) [31]. This imposes a restriction on the temperature range over which electrolysis experiments can be done. In order to have calcium chloride molten at low temperatures, it was mixed with sodium chloride with which it forms a eutectic at about 48% (mole NaCl) composition. From phase diagram of $CaCl_2$-NaCl system shown in Figure 3.8, it can be seen that operating temperature of the cell has to be above 504°C.

In the following experiments $CaWO_4$ was used as the cathode material and $CaCl_2$-NaCl salt mixture with eutectic composition was used as the electrolyte (See Chapter 3 for the details of the experiments). The results of the experiments showed that it was possible to produce tungsten with this setup, but in addition

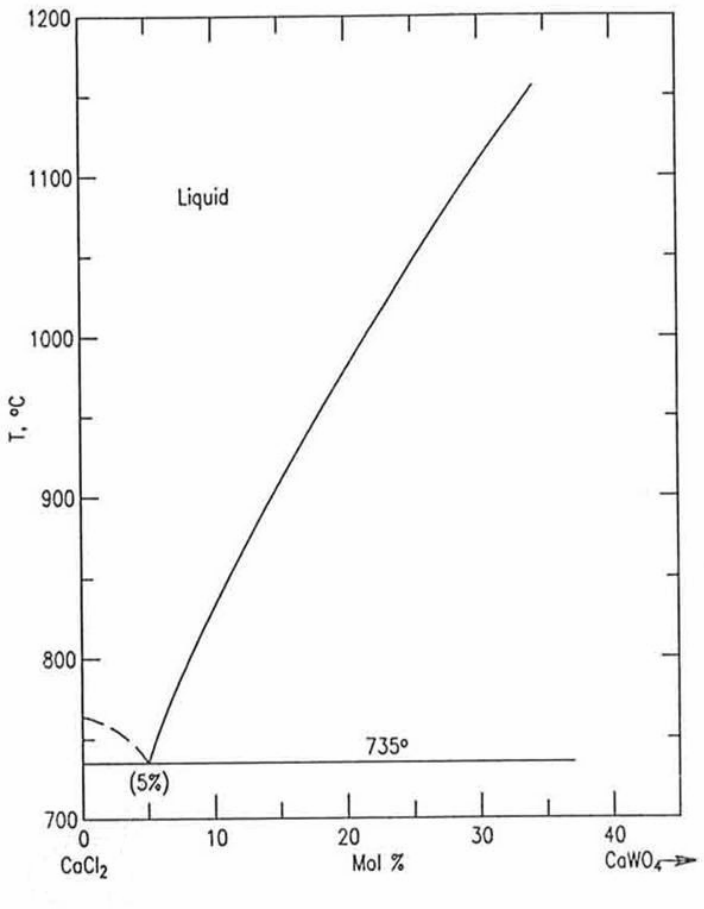


Figure 4.6:$CaCl_2$-$CaWO_4$ Phase Diagram (Reproduced from [31])

to tungsten there were significant amounts of calcium carbonate ($CaCO_3$) and calcium hydroxide ($Ca(OH)_2$). These compounds were formed after electrolysis experiments either inside the cell vessel or during washing stage of the cathode by water. X-ray diffraction result of one of the experiments is given in Figure 4.7. In this experiment, temperature was 600°C and the applied potential was 2.8 volts.

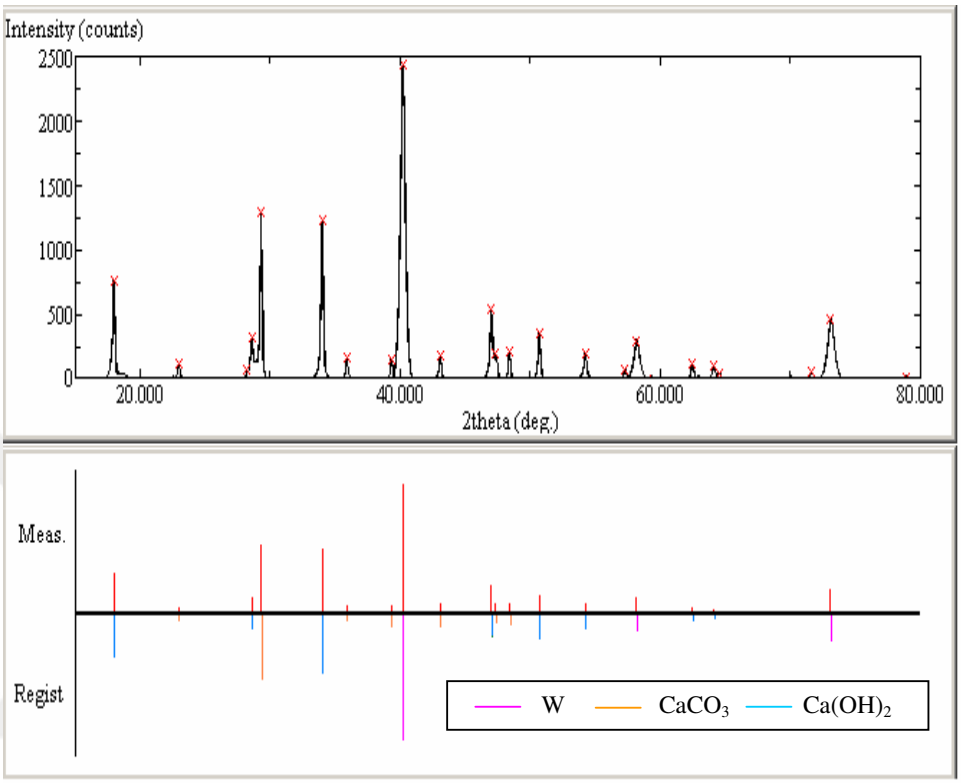


Figure 4.7: X-ray diffraction spectrum of one of the experiments with $CaWO_4$ pellet in $CaCl_2$-NaCl molten eutectic mixture. Products are W, $CaCO_3$ and $Ca(OH)_2$.

4.2.2 Effect of Sintering

As it was mentioned in section 3.2.1, the pellets were prepared according to two different routes in order to examine the effect of sintering on the electrolysis of $CaWO_4$. Current versus time graphs of two experiments are given in Figure 4.8. In one of the experiments the pellet was sintered at 1200°C and in the other one the pellet was not sintered at all. In both experiments, pellets were identical in geometry and mass, temperature was 600°C and the applied potential was 2.8 volts. As it can clearly be seen, higher current values were recorded with the unsintered pellet. It was observed that tungsten formation occurred only at the surfaces of the pellets which were sintered at 1200°C (Figure 4.9). Reduction did

not occur in the interior parts and $CaWO_4$ was left unreacted at these regions (Figure 4.10). On the other hand, only mechanically pressed and heated pellets were distorted significantly and reduced completely to tungsten (Figure 4.7).

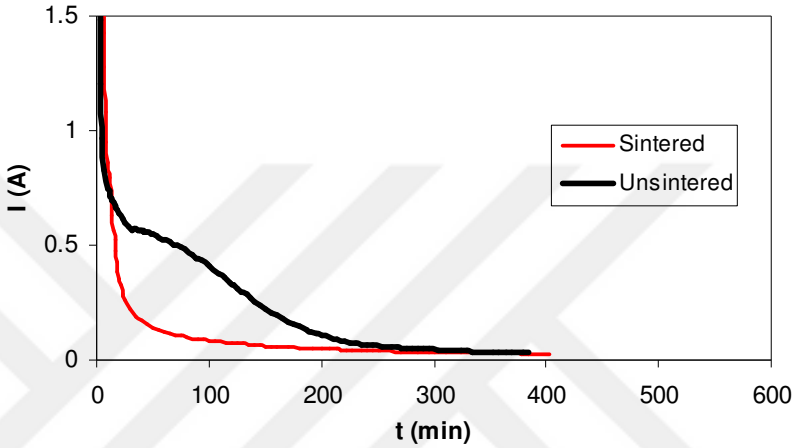


Figure 4.8: Current vs. Time Graphs of the Experiments (Higher current values were recorded with the unsintered pellet.)

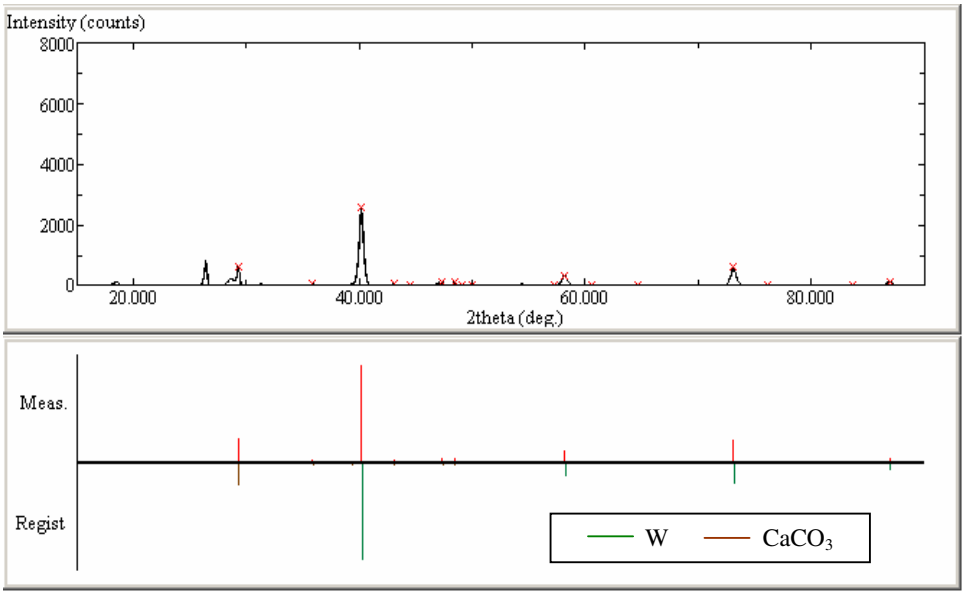


Figure 4.9: X-ray diffraction spectrum of a sample (sintered at 1200°C) after 400 minutes of electrolysis. The sample was taken from the surface.

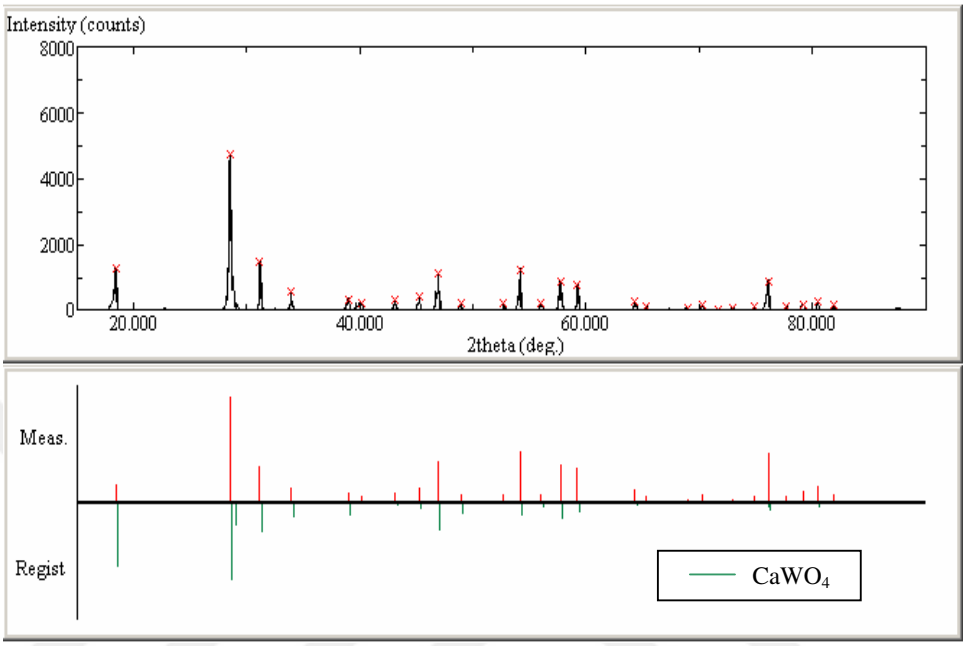


Figure 4.10: X-ray diffraction spectrum of a sample (sintered at 1200°C) after 400 minutes of electrolysis. The sample was taken from the interior parts of the pellet.

As it is apparent from the above discussion, use of unsintered pellets demonstrates a clear advantage. Therefore in the following experiments unsintered $CaWO_4$ pellets were used as the starting material for the electrolysis.

4.2.3 Determination of Theoretical Potential for the Reduction Reaction

In real systems, observed cell potential may deviate largely from the theoretical potential required for the reduction reaction. There will be additional potentials due to the overvoltages and the resistances of the cell and the electrical connections when current is passing through the cell. Total applied potential for the present study can be given as:

$$E_{applied} = E_{reaction} + E_{electrical\ connections} + E_{electrolyte} + E_{pellet} + \eta$$

where; $E_{reaction}$ is the theoretical potential required for the reduction reaction.

$E_{electrical\ connections}$ is the voltage drop along the electrical connections ($E_{electrical\ connections}=I\times R_{electrical\ connections}$).

$E_{electolyte}$ is the electrolyte ohmic voltage ($E_{electolyte}=I\times R_{electrolyte}$).

E_{pellet} is the pellet ohmic voltage ($E_{pellet}=I\times R_{pellet}$).

η is the anodic and cathodic overvoltages. For the present study it may be considered to be mainly due to CO_2 evolution at the anode.

When there is no current passing, ohmic voltages due to resistance will be zero. Therefore, it is clear from the above expression that extrapolation of voltage vs. current (E vs. I) curve to zero current should give the theoretical potential required for the reduction reaction plus the anodic overvoltage ($E_{reaction}+\eta$). Furthermore, if the voltage drops along the electrical connections (which were already measured, see section 3.2.2) are subtracted from the applied potentials, the slope of this E vs. I curve will give the resistance of the pellet and the electrolyte ($R_{pellet}+R_{electrolyte}$). It should be noted that current dependence of overvoltage is logarithmic and small within the range of current values used and can be neglected for computational purposes.

4.2.3.1 Experiments at Applied Constant Potential

In the light of above information, experiments were conducted at different applied constant potentials and corresponding current values as a function of time were recorded. The results are given in Figure 4.11. Net cell voltages (E_{net}) were obtained by subtracting voltage drops along the electrical connections ($E_{electrical\ connections}$) from the applied potentials ($E_{applied}$).

$$E_{net} = E_{applied} - E_{electrical\ connections}$$

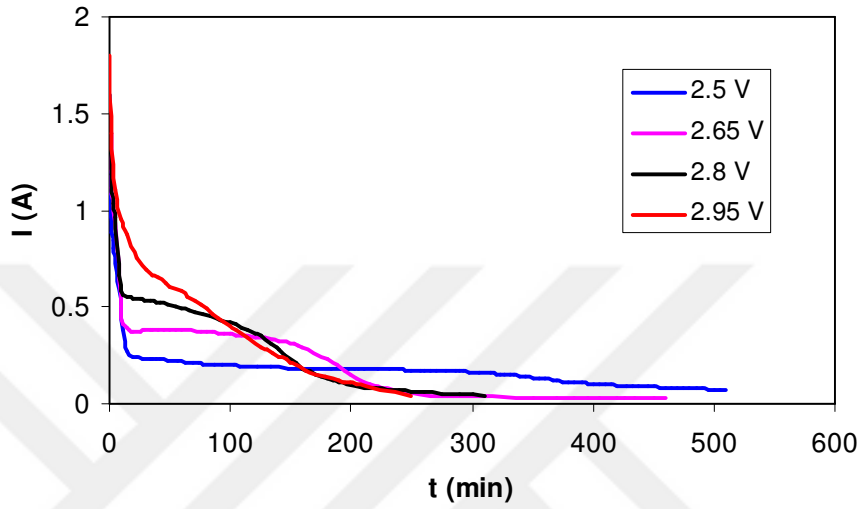


Figure 4.11: I vs. t Curves of Electrolysis of $CaWO_4$ Pellets at Different Applied Constant Voltages

Corresponding current values to these net cell voltages were chosen according to the electrical charge passed through the system. In each experiment, the current value corresponding to the passage of 0.035 Faradays (3377.5 Coulombs) of electrical charge was selected. This corresponds to completion of about 68% of reduction. Therefore, the moment at which the current value was taken, differed from one experiment to the other. Table 4.1 gives the list of the calculated values and also the corresponding minutes of the experiments at which the current values were taken. In the calculations, current was used instead of current density, because the pellets were identical in all of the experiments. Figure 4.12 shows the variation of current with the applied net cell voltage. Extrapolation of the regression line to zero current gave a potential value of 2.26 V ($E_{reaction}+\eta$), and the slope of the line was calculated as 0.91 ohm ($R_{pellet}+R_{electrolyte}$).

Table 4.1: List of Calculated Values

$E_{applied}$ (V)	$E_{electrical\ connections}$ (V)	E_{net} (V)	I (A)	Corresponding time (min)
2.5	0.07	2.43	0.18	257^{th}
2.65	0.13	2.52	0.33	140^{th}
2.80	0.17	2.63	0.41	105^{th}
2.95	0.22	2.73	0.51	70^{th}

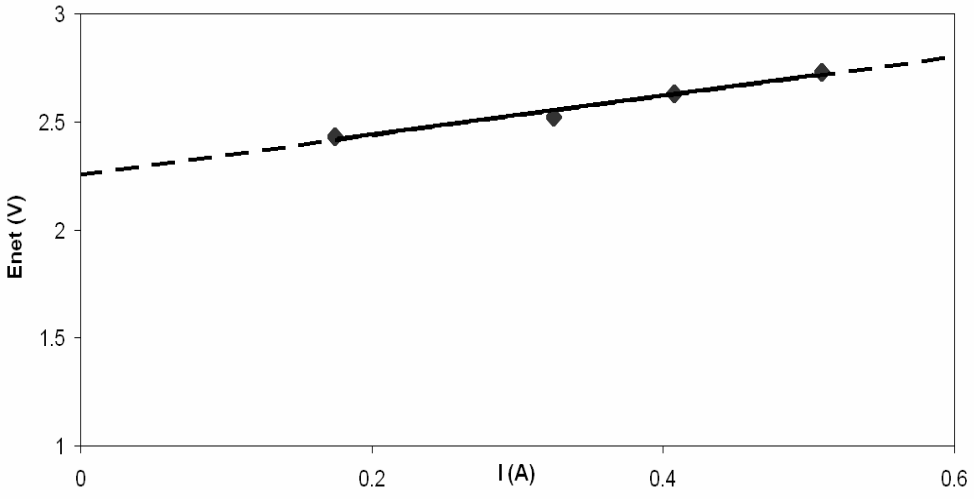


Figure 4.12: Variation of Current Values with Net Cell Potential (Extrapolation of the regression line gives $E_{reaction}+\eta$, and the slope of the line gives $R_{pellet}+R_{electrolyte}$.)

As it can be seen from Figure 4.11, higher current values were recorded at the initial periods of the experiments. This is most probably because electroreduction of the pellet starts from the regions at which $CaWO_4$ pellet is in contact with the stainless steel current collector and then proceeds to the inner regions. In Figure 4.13, a photograph of a partially reduced pellet is given.



Figure 4.13: Photograph of A Partially Reduced Sample (Black regions are the reduced portions, whereas white regions are the unreduced portions of the pellet.)

Black regions are the reduced portions, whereas white regions are the unreduced portions of the pellet. With reference to Figure 4.13, it can be said that the reduction started from the bottom of the pellet where it is in contact with the current collector (stainless steel spoon in the photograph) and proceeded to the upper surface. Only the white portions seen on the upper surface were left unreacted. This figure can also be considered as an indication that the reaction

starts where the pellet is in contact with the current collector. As a result, rapid decrease of the current values in the experiments, which is evident from Figure 4.11, could be attributed to the resistance of the pellet. Furthermore, it can be told that the current values used in Figure 4.12, were taken soon enough to include resistance of the pellet in the slope of the regression line.

From the above discussion, it can be concluded that pellet resistance does not play an important role during the initial periods of the experiments. Therefore, if the E_{net} vs. I curve is plotted for the initial minutes of the experiments, slope of the regression line should give the resistance of electrolyte only ($R_{electrolyte}$). In order to verify this conclusion, current values, corresponding to the passage of 0.0052 Faradays (502.6 Coulombs) of electrical charge, were plotted as a function of applied net cell voltages (Figure 4.14). This corresponds to completion of about 10% of reduction. List of calculated values are given in Table 4.2. Slope of the regression line was calculated as 0.35 ohm ($R_{electrolyte}$). In the literature specific resistance of $CaCl_2$-NaCl eutectic salt mixture is given in the range 0.68-0.81 (ohm.cm) [32]. Specific resistance of the electrolyte can be calculated from the formula:

$$\rho = R \times \frac{A}{l}$$

where; ρ is the specific resistance, R is the resistance, A is the cross sectional area of the cathode (1.91 cm^2) and l is the anode-cathode distance (1 cm). From this formula, specific resistance of the electrolyte was calculated as 0.67 (ohm.cm), which shows approximately 8 % deviation from the average value given in the literature. Furthermore, extrapolation of the regression line to zero current yields 2.22 V potential difference, a value very close to 2.26 V obtained from the previous diagram.

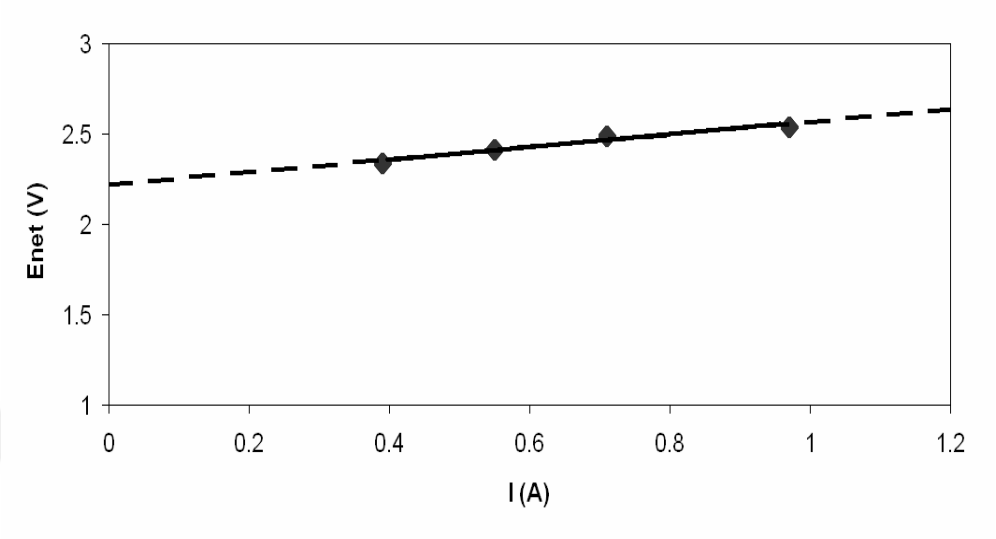


Figure 4.14: E_{net} vs. I Curve for the Initial Periods of the Experiments (Slope of the regression line gives the resistance of the electrolyte.)

Table 4.2: List of Calculated Values

$E_{applied}$ (V)	$E_{electrical\ connections}$ (V)	E_{net} (V)	I (A)	Corresponding time (min)
2.5	0.16	2.34	0.39	12^{th}
2.65	0.24	2.41	0.55	9^{th}
2.80	0.31	2.49	0.71	8^{th}
2.95	0.41	2.54	0.97	6^{th}

4.2.3.2 Experiments at Applied Constant Current

Further experiments were conducted to test the results of the study given in section 4.2.3.1 at different applied constant current values. Variations of the observed potential values with time were recorded and given in Figure 4.15. Similarly, rapid increase of the voltage values is most likely due to the resistance of the pellet, which becomes more important as the direct contact between the pellet and the current collector gets looser. It is clear that subtraction of E_{pellet}, $E_{electrolyte}$ and $E_{electrical\ connections}$ from the observed potential $E_{observed}$, should give $E_{reaction}+\eta$ value. However, Figure 4.15 needed to be modified in order to have the amount of electrical charge passed equal in all the experiments at the same horizontal axis. Since current is the rate of flow of electrical charge ($q=I\times t$), time axes of the experiments were substituted with electrical charge (q). Figure 4.16 shows the observed potential values as a function of electrical charge passing through the system.

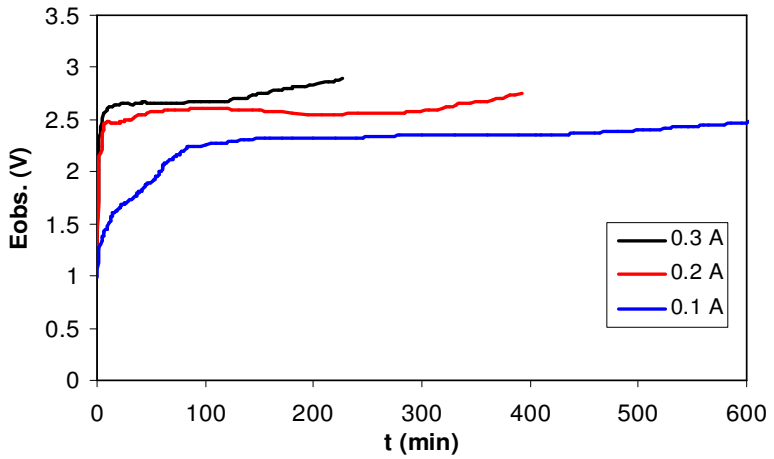


Figure 4.15: Observed Potential Values As a Function of Time at Different Applied Constant Current Values

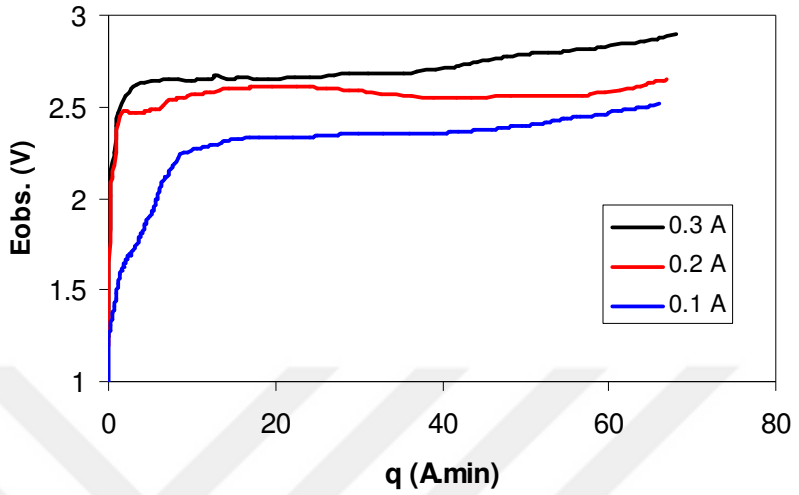


Figure 4.16: Observed Potential Values As a Function of Electrical Charge at Different Applied Constant Current Values

A list of calculated values is given in Table 4.3. Observed potential values were selected according to the passage of 0.025 Faradays (2400 Coulombs) of electrical charge through the system. This corresponds to completion of nearly 50% reduction. In order to determine $E_{pellet}+E_{electrolyte}$, $R_{pellet}+R_{electrolyte}$ value (0.91 ohm) obtained in section 4.2.3.1 was used. As it can be seen from Table 4.3, subtraction of $E_{electrical\ connections}$, E_{pellet} and $E_{electrolyte}$ from the observed potential $E_{observed}$, gave consistent $E_{reaction}+\eta$ values with the ones found in section 4.2.3.1.

Table 4.3 : List of Calculated Values

I (A)	$E_{observed}$ (V)	$E_{electrical\ connections}$ (V)	$E_{electrolyte}+E_{pellet}$ (V)	$E_{reaction}+\eta$ (V)
0.1	2.35	0.03	0.091	2.23
0.2	2.55	0.08	0.182	2.29
0.3	2.70	0.12	0.273	2.31

4.2.4 Determination of Electroreduction Pathway

Some of the possible reactions that can occur in such a system and their corresponding standard potential values at 600°C are given below [30]:

When the anodic gaseous product is a mixture of CO_2 and Cl_2;

$CaWO_4(s) + C(s) + CaCl_2(l) = W(s) + 2CaO(s) + CO_2(g) + Cl_2(g)$ $E° = -0.85$ V (Rxn 1)

$CaWO_4(s) + 2C(s) + CaCl_2(l) = W(s) + 2Ca(s) + 2CO_2(g) + Cl_2(g)$ $E° = -1.22$ V (Rxn 2)

$CaWO_4(s) + 1/2C(s) + CaCl_2(l) = 2\,Ca(s) + WO_3(s) + 1/2CO_2(g) + Cl_2(g)$ $E° = -3.00$ V (Rxn 3)

$2CaWO_4(s) + C(s) + CaCl_2(l) = Ca_3WO_6(s) + W + Cl_2(g) + CO_2(g)$ $E° = -0.80$ V (Rxn 4)

$Ca_3WO_6(s) + C(s) + CaCl_2(l) = W(s) + 4CaO(s) + CO_2(g) + Cl_2(g)$ $E° = -0.90$ V (Rxn 5)

$Ca_3WO_6(s) + 3C(s) + CaCl_2(l) = W(s) + 4Ca(s) + 3CO_2(g) + Cl_2(g)$ $E° = -1.41$ V (Rxn 6)

$Ca_3WO_6(s) + 3/2C(s) + CaCl_2(l) = 4Ca(s) + WO_3 + 3/2CO_2(g) + Cl_2(g)$ $E° = -2.44$ V (Rxn 7)

When the anodic gaseous product is CO_2;

$CaWO_4(s) + 3/2\ C(s) = W(s) + CaO(s) + 3/2CO_2(g)$ $E° = -0.31$ V (Rxn 8)

$CaWO_4(s) + 1/2C(s) = Ca(s) + WO_3(s) + 1/2CO_2(g)$ $E° = -2.60$ V (Rxn 9)

$CaWO_4(s) + 2C(s) = Ca(s) + W + 2CO_2(g)$ $E° = -0.68$ V (Rxn 10)

$CaO(s) + 1/2C(s) = Ca(s) + 1/2CO_2(g)$ $E° = -1.80$ V (Rxn 11)

$Ca_3WO_6(s) + 3/2\ C(s) = W(s) + 3CaO(s) + 3/2CO_2(g)$ $E° = -0.37$ V (Rxn 12)

$Ca_3WO_6(s) + 3C(s) = W(s) + 3Ca(s) + 3CO_2(g)$ $E° = -1.08$ V (Rxn 13)

$Ca_3WO_6(s) + 3/2C(s) = 3Ca(s) + WO_3(s) + 3/2CO_2(g)$ $E° = -2.11$ V (Rxn 14)

When the anodic gaseous product is Cl_2;

$CaCl_2(l) = Ca(s) + Cl_2(g)$ $E° = -3.40$ V (Rxn 15)

$NaCl(l) = Na(s) + 1/2\ Cl_2(g)$ $E° = -3.37$ V (Rxn 16)

$CaWO_4(s) + 3CaCl_2(l) = W(s) + 4CaO(s) + 3Cl_2(g)$ $E° = -1.92$ V (Rxn 17)

$Ca_3WO_6(s) + 3CaCl_2(l) = W(s) + 6CaO(s) + 3Cl_2(g)$ $E° = -1.97$ V (Rxn 18)

When the anodic gaseous product is O_2:

$CaWO_4(s) = W(s) + CaO(s) + 3/2\ O_2(g)$ $E° = -1.33$ V (Rxn 19)

$CaWO_4(s) = Ca(s) + WO_3(s) + 1/2O_2(g)$ $E° = -3.62$ V (Rxn 20)

$CaWO_4(s) = Ca(s) + W(s) + 2O_2(g)$ $E° = -1.70$ V (Rxn 21)

$CaO(s) = Ca(s) + 1/2\ O_2(g)$ $E° = -2.82$ V (Rxn 22)

$Ca_3WO_6(s) = W(s) + 3CaO(s) + 3/2\ O_2(g)$ $E° = -1.33$ V (Rxn 23)

$Ca_3WO_6(s) = 3Ca(s) + WO_3(s) + 3/2O_2(g)$ $E° = -3.14$ V (Rxn 24)

$Ca_3WO_6(s) = 3Ca(s) + W(s) + 3O_2(g)$ $E° = -2.10$ V (Rxn 25)

When the anodic gaseous products is a mixture of Cl_2 and O_2;

$CaWO_4(s) + CaCl_2(l) = W(s) + 2CaO(s)$ $E° = -1.52$ V (Rxn 26)
$+ Cl_2(g) + O_2$

$CaWO_4(s) + CaCl_2(l) = 2Ca(s) + WO_3(s)$ $E° = -3.51$ V (Rxn 27)
$+ 1/2O_2(g) + Cl_2(g)$

$CaWO_4(s) + CaCl_2(l) = W(s) + 2Ca(s)$ $E° = -2.04$ V (Rxn 28)
$+ 2O_2(g) + Cl_2(g)$

$Ca_3WO_6(s) + CaCl_2(l) = W(s) + 4CaO(s)$ $E° = -1.58$ V (Rxn 29)
$+ Cl_2(g) + O_2$

$Ca_3WO_6(s) + CaCl_2(l) = 4Ca(s) + WO_3(s) + 3/2O_2(g) + Cl_2(g)$ $E° = -3.21$ V (Rxn 30)

$Ca_3WO_6(s) + CaCl_2(l) = W(s) + 4Ca(s) + 3O_2(g) + Cl_2(g)$ $E° = -2.29$ V (Rxn 31)

In the experiments, it was realized that a significant amount of chlorine gas was released in spite of the fact that the applied potentials were too low for $CaCl_2$ and/or NaCl decomposition. Also, presence of $CaCO_3$ in the X-ray diffraction results of the reduced specimens (Figure 4.7) could only be explained by the evolution of CO_2 at the anode. Therefore, it has been thought that, among these reactions, the ones having CO_2 and Cl_2 as the anodic products are most likely to occur during electrolysis.

In section 4.2.2, $E_{reaction}+\eta$ value was calculated as approximately 2.27 V (average of the results found in sections 4.2.3.1 and 4.2.3.2). Therefore, among the reactions having CO_2 and Cl_2 as the anodic products, reactions 3 and 7 cannot take place.

Furthermore, with reference to Figure 4.7, the proposed reaction(s) should give W and Ca or CaO as the reaction products. Presence of $CaCO_3$ and $Ca(OH)_2$, which are seen in Figure 4.7, can be explained by the reactions of Ca or CaO with CO_2 and H_2O as will be explained in detail in section 4.2.5.

Concerning these constraints, it can be proposed that Rxn 1 alone, Rxn 2 alone or Rxn 4 followed by one of the reactions; Rxn 5, Rxn6, Rxn 12, Rxn 13, Rxn 14, Rxn 18, Rxn 23, Rxn 25, Rxn 29 or Rxn 31 could be occurring during electrolysis. However, except at very early stages, there is no indication that the reaction mechanism involves more than one step. Voltage values recorded during the experiments were quite stable and did not show any fluctuations.

Furthermore, X-ray diffraction results of partially reduced samples, which were prepared by terminating the reduction before completion, did not show the presence of any Ca_3WO_6.

More precise estimations could be done on the reduction mechanism, if the CO_2 overvoltage on graphite anode in $CaCl_2$ – NaCl molten salt solutions at 600°C was known exactly. There are not sufficient data in the literature about the value of this overvoltage especially at low temperatures. Overvoltage data are usually presented as Tafel plots.

$$\eta = a + b \log i$$

where a and b are the Tafel coefficients and i is the anodic current density ($\frac{\text{current}}{\text{anode area}}$). Table 4.4 shows Tafel coefficients, which were found in literature, for anodic overvoltage on graphite in cryolite melts for two different temperatures [34].

Table 4.4: Tafel Coefficients for Anodic Overvoltage on Graphite in Cryolite Melts for Two Different Temperatures [34]

Temperature (°C)	Tafel Range ($A.cm^{-2}$)	a (V)	b (V)
1000	0.05 – 0.8	0.52	0.4
790	0.01 – 1	0.60	0.22

From this data, η values were calculated for an anodic current density of 0.1 ($A.cm^{-2}$), which was within the range of current values used in this study (anode area was 1.33 cm^2). Figure 4.17 shows the resulting T vs. η graph. Extrapolation of the regression curve to 600°C gave an η value of 1.1 V. Exponential type regression was used because of Arrhenius type temperature dependency of overvoltage.

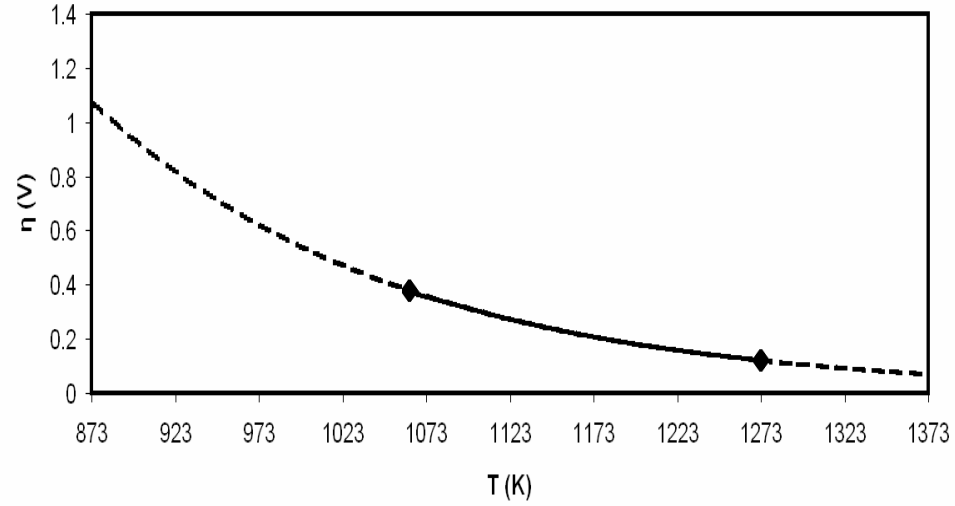


Figure 4.17: T vs. η Graph Obtained for an Anodic Current Density of 0.1 A.cm^{-2} (Extrapolation of the regression curve to 600°C gives an η value of 1.1 V.)

It should be noted that the values in Table 4.4 were given for cryolite melts in aluminum production. Furthermore, in aluminum production the anodic gaseous product is a mixture of CO_2 and CO as a result of higher temperatures. Finally two points are not sufficient to do a regression as the one given in Figure 4.17. Nevertheless, the above study gives an idea about how important can the anodic overvoltage be at low temperatures. Therefore, Rxn 1 or Rxn 2 may be considered to be electroreduction pathway of $CaWO_4$ reduction in this study.

4.2.5 Isolation of Tungsten

As it can be seen from Figure 4.7, in addition to tungsten, the reduced specimen contains significant amounts of $CaCO_3$ and $Ca(OH)_2$. These compounds were formed after electrolysis experiments either inside the cell vessel or during washing stage of the cathode by water. The proposed reactions in section 4.2.4, contains Ca or CaO as the electrolysis products as well as tungsten. Presence of

$CaCO_3$ can be explained by the reaction of one of these compounds with the anodic gaseous product CO_2. The reactions are given below:

$CaO(s) + CO_2(g) = CaCO_3(s)$
$Ca(s) + 3/2CO_2(g) = CaCO_3(s) + 1/2C(s)$

Furthermore, if any Ca or CaO were left unreacted, they react with water at the washing stage after the experiment (see section 3.2.2 for the details of washing stage) to form $Ca(OH)_2$. The reactions are given below:

$CaO(s) + H_2O(l) = Ca(OH)_2(s)$
$Ca(s) + 2H_2O(l) = Ca(OH)_2(s) + H_2(g)$

Argon flushing was performed to prevent the reaction between Ca/CaO and CO_2 in the subsequent experiments. Consequently, formation of $CaCO_3$ was inhibited with the removal of CO_2 from the cell vessel by argon flushing at the end of the experiment. Then all the Ca or CaO reacted with water to form $Ca(OH)_2$ as expected. Figure 4.18 shows the X-ray diffraction spectrum of a sample after an experiment in which the vessel was flushed with argon gas.

The last step to isolate tungsten was the removal of $Ca(OH)_2$ and this was achieved by treating the sample with a dilute hydrochloric (HCl) acid solution. It was observed that tungsten was sufficiently inert in such a solution, whereas $Ca(OH)_2$ and/or CaO can easily and completely be removed. Figure 4.19 shows the X-ray diffraction result of a cathode sample after 0.2 M HCl solution treatment.

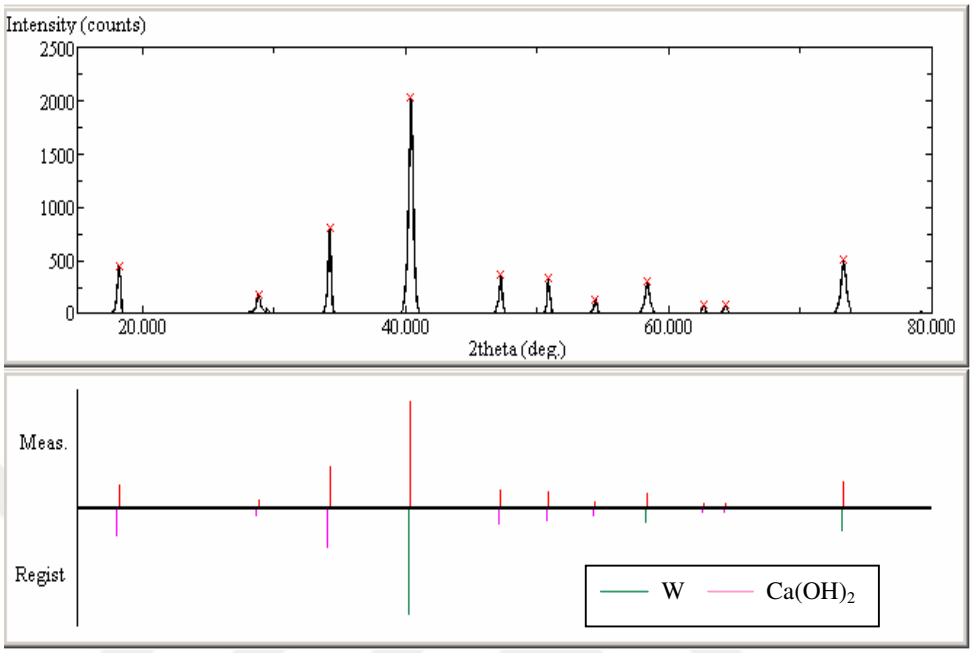


Figure 4.18: X-ray diffraction spectrum of a sample after an experiment in which the vessel was flushed with argon gas.

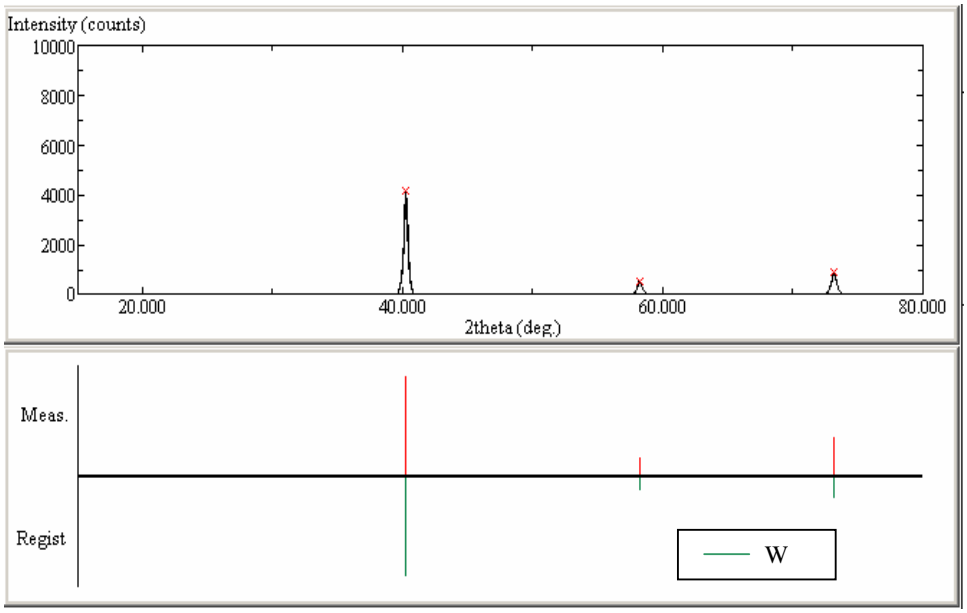


Figure 4.19: X-ray Diffraction Spectrum of a Sample after 0.2 M HCl Solution Treatment

CHAPTER 5

CONCLUSION

The objective of this research was to produce tungsten from tungsten compounds by electrodeoxidation in molten salt media. Preliminary experiments indicated that tungsten could be produced by electrodeoxidation of tungsten trioxide (WO_3) in calcium chloride ($CaCl_2$) molten salts at 900°C. However, there were significant amounts of tungsten losses due to formation of volatile tungsten oxychloride (WO_2Cl_2) when WO_3 comes in contact with $CaCl_2$ inside the cell vessel. Thermodynamic computations were used to support this result.

Electrodeoxidation of synthetic calcium tungstate ($CaWO_4$) was performed by using NaCl - $CaCl_2$ (48% mole NaCl) eutectic salt mixture at 600°C. X-ray diffraction results of electrodeoxidized $CaWO_4$ demonstrated that metallic tungsten could be obtained by this method. However, in addition to tungsten there were significant amounts of calcium compounds in the reduced samples.

In the experiments involving the study of the sintering effect on $CaWO_4$ reduction, higher current values were recorded with the unsintered pellets. It was also found that, the unsintered pellets were reduced completely to tungsten, whereas tungsten formation occurred only at the surfaces of the sintered pellets. Reduction did not occur in the inner regions of the pellets and $CaWO_4$ was left unreacted at these regions.

Computations indicated that a potential difference of approximately 2.27 V makes up the sum of theoretical voltage and overpotential, except at very early stages of $CaWO_4$ reduction in the present study.

In order to isolate tungsten from the other electrolysis products reduced samples were treated with dilute HCl solutions. It was observed that tungsten was sufficiently inert in such a solution, whereas calcium oxide (CaO) and/or calcium hydroxide ($Ca(OH)_2$) could easily and completely be removed.

Future work may involve determination of the exact pathway of electroreduction and optimization of electrolysis conditions. Direct use of the so called mineral scheelite ($CaWO_4$) instead of synthetically produced $CaWO_4$ could be tested. If tungsten could be produced from scheelite mineral, many intermediate steps in today's tungsten production method could be eliminated.

REFERENCES

[1] ITIA: Tungsten properties,
[http://www.itia.org.uk/Default.asp?page=33],
Last Accessed: January 2007.

[2] ITIA: Tungsten uses,
[http://www.itia.org.uk/Default.asp?page=34],
Last Accessed: January 2007.

[3] Primary Metals Inc.,
[http://www.primarymetals.ca/tungstenuses.htm],
Last Accessed: January 2007.

[4] Primary Metals Inc.,
[http://www.primarymetals.ca/images/graphs/production_lg.jpg],
Last Accessed: January 2007.

[5] Lassner E., and Schubert W.D., "Tungsten Properties, Chemistry, Technology of the Element, Alloys, and Chemical Compounds", p. 81, (1999) Kluwer Academic / Plenum Publishers, New York.

[6] Lassner E., and Schubert W.D., "Tungsten Properties, Chemistry, Technology of the Element, Alloys, and Chemical Compounds", p. 397, (1999) Kluwer Academic / Plenum Publishers, New York.

[7] ITIA: Tungsten prices,
[http://www.itia.org.uk/Default.asp?page=40],
Last Accessed: January 2007.

[8] ITIA: Tungsten Minerals & Deposits,
[http://www.itia.org.uk/Default.asp?page=49],
Last Accessed: January 2007.

[9] ITIA: Tungsten reserves,
[http://www.itia.org.uk/Default.asp?page=51],
Last Accessed: January 2007.

[10] Aydoğanlı E., "Türkiye Volfram Envanteri", p. 30, (1978) Maden Tetkik ve Arama Enstitüsü Yayınlarından No: 170.

[11] ITIA: Tungsten processing,
[http://www.itia.org.uk/Default.asp?page=38],
Last Accessed: January 2007.

[12] ITIA: Intermediates,
[http://www.itia.org.uk/Default.asp?page=39],
Last Accessed: January 2007.

[13] Rosenqvist T., "Thermochemical Data for Metallurgists", p. 55, (1970) Tapir.

[14] Ward R. G., and Hoar T. P., *J. Inst. Met.*, **vol. 90** (1961), p. 6.

[15] Okabe T. H., Suzuki R. O., Oishi T., and Ono K., *Tetsuto-Hagane* (*J. Iron Steel Inst. Japan*), **vol. 77** (1991), p. 93.

[16] Okabe T. H., Oishi T., and Ono K., *J. Alloy Comp.*, **vol. 184** (1992), p. 43.

[17] Okabe T. H., Ikezawa M., Suzuki R. O., Oishi T., and Ono K, *CAMP ISIJ* (Proc *Annual Meeting of the Iron and Steel Institute of Japan*), **vol. 3** (1990), p. 101.

[18] Chen G. Z., and Fray D. J., *J. Appl. Electrochem.*, **vol. 31** (2001), p. 155.

[19] Chen G. Z., Fray D. J., and Farthing T. W., *Metall. Mater. Trans. B*, **vol. 32** (2001), p. 1041.

[20] Chen G.Z., Fray D. J., and Farthing T.W., *Nature*, **vol. 407** (2000), p. 361.

[21] Chen G. Z., Fray D. J., and Gordo E., *JOM*, **vol. 56** (2004), p. 138.

[22] Jin X., Gao P., Wang D., Hu X., and Chen G. Z., *Angew. Chem.*, **vol. 43** (2004), p. 733.

[23] Han W. K., Choi J. W., Hwang G. H., Hong S. J., Lee J. S., and Kang S. G., *Appl. Surf. Sci.*, **vol. 252** (2006), p. 2832.

[24] Chen G. Z., and Fray D. J., in *Progress in Molten Salt Chemistry 1*,(eds) Berg R.W. and Hjuler H. A., Elsevier, Paris (2000), p.157.

[25] Chen G. Z., and Fray D. J., *Light Metals 2001*, (ed) Anjier J L, Warrandale, PA,TMS, (2001) p. 1147.

[26] Yan X.Y., and Fray D. J., *Metall. Mater. Trans. B*, **vol. 33** (2002), p. 685.

[27] Dring K., Bhagat R., Jackson M., Dashwood R., and Inman D., *J. Alloy Comp.*, **vol. 419** (2006), p.103.

[28] Karakaya İ., "Electrochemical Determination of Thermodynamic Properties of Magnesium Cell Electrolyte the System $MgCl_2$-NaCl-$CaCl_2$", (1985) Dept. of Mining and Metallurgical Eng., McGill University, Ph. D.

[29] Collection of Phase Diagrams,
[http://www.crct.polymtl.ca/fact/phase_diagram.php?file=CaCl2-NaCl.jpg&dir=FTsalt],
Last Accessed: January 2007.

[30] FACT – Facility for the Analysis of Chemical Thermodynamics,
[http://www.crct.polymtl.ca/fact/],
Last Accessed: January 2007.

[31] Mchale A. E., "Phase Diagrams for Ceramists", p. 129, (Annual'91) The American Soc., Inc.

[32] Strelets Kh. L., "Electrolytic Production of Magnesium", p. 199, (1977) Keter Publishing House Jerusalem Ltd.

[33] Grjotheim K., Krohn C., Malinovskỳ M., Matiašovskỳ K., Thonstad J., "Aluminum Electrolysis", p. 211, (1977) Aluminum – Verlag GmbH·Düsseldorf